CZECH TECHNICAL UNIVERSITY IN PRAGUE

FACULTY OF MECHANICAL ENGINEERING

DOCTORAL THESIS STATEMENT

Czech Technical University in Prague
Faculty of Mechanical Engineering
Department of Fluid Dynamics and Thermodynamics

Doctoral Thesis Statement

Compressible Fluid Flow through Narrow Channels

Jindřich Hála

Doctoral Study Programme: Mechanical Engineering

Study Field: Thermomechanics and Fluid Mechanics

Supervisor: Prof. Ing. Pavel Šafařík, CSc.

Doctoral thesis statement for obtaining the academic title of "Doctor" abbreviated to "Ph.D."

Praha April 2021

Title in Czech: Proudění vazké stlačitelné tekutiny úzkými kanály

This doctoral thesis is an outcome of a part-time doctoral study programme at the Department of Fluid Mechanics and Thermodynamics, Faculty of Mechanical Engineering, Czech Technical University in Prague.

Dissertant: Ing. Jindřich Hála
Department of Fluid Mechanics and Thermodynamics
Faculty of Mechanical Engineering
CTU in Prague

Supervisor: Prof. Ing. Pavel Šafařík, CSc.
Department of Fluid Mechanics and Thermodynamics
Faculty of Mechanical Engineering
CTU in Prague

Advisor: Doc. Ing. Martin Luxa, Ph.D.
Institute of Thermomechanics of the Czech Academy of Sciences

Reviewers:

The thesis statements were set out on:

The defence of the dissertation thesis will take place on ..... at .....
in room Nr. ..... at the Faculty of Mechanical Engineering, CTU in Prague, Technická 4, Prague 6.
The thesis is available at the Department of Fluid Mechanics and Thermodynamics, Faculty of Mechanical Engineering, CTU in Prague, Technická 4, Prague 6.

Head of Doctoral Study Field Thermomechanics and Fluid Mechanics

Faculty of Mechanical Engineering, CTU in Prague

Abstract

Title: Compressible Fluid Flow through Narrow Channels

The turbulence transition in pipe and channel flow represents up to now an important topic, since it is the nature of the flow, which substantially affects the friction and associated losses. With increasing miniaturization and more detailed numerical simulations of the various small flow parts of the turbomachines, the need for experimental data to explore the narrow channel flow phenomena and to validate numerical codes is still there.

This thesis presents the results of the project which aimed to experimentally and numerically explore the compressible viscous flow in narrow channels of the rectangular cross-section of the high aspect ratio. Main objectives of this work were to explore the nature of the flow in such channels using a number of experimental methods including hot-film probe, explore the influence of two types of surface roughness and discuss the effects associated with the phenomenon of aerodynamic choking due to friction. Apart from the narrow channel measurements, the thesis contains also the detailed description of the calibration process of the hot-film probe and accompanying numerical study.

It was observed that despite the channel length to channel height ratio ranging from 50 to 200, the flow was mostly transitional except the flow in the smallest channel of the height $h = 0.5\,\mathrm{mm}$. The effects of the surface roughness were explored using both qualitative and quantitative measurements by means of hot-film probe. The later provided distribution of the wall shear stress at five locations along the channel for two chosen regimes. Further, the analysis revealed inapplicability of the one-dimensional theory for the estimation of the friction factor. The theoretical analysis of the flow choking supported by numerical simulations shows that due to frictional losses, the actual choking is shifted towards the lower back pressure ratios. These findings were summarized in charts, which comprehensively illustrate derived relations.

Keywords

narrow channel flow, minichannel, compressible flow, wall shear stress, hot-film anemometry

Anotace

Název: Proudění vazké stlačitelné tekutiny úzkými kanály

Přechod do turbulence v trubkách a kanálech nekruhových průřezů stále představuje aktuální problém dynamiky tekutin, jelikož je to právě režim proudění, který zásadně ovlivňuje tření a s ním spojené ztráty. S pokračující miniaturizací a stále detailnějšími numerickými simulacemi i malých průtočných částí turbostrojů vyvstává potřeba prozkoumat jevy, ke kterým dochází při proudění v takto úzkých kanálech a získat data, na jejichž základě by bylo možné validovat numerické modely.

Tato práce představuje výsledky doktorandského projektu, který měl za cíl pomocí experimentů a numerické simulace prozkoumat proudění vazké stlačitelné tekutiny úzkými kanály obdélníkového průřezu s vysokým poměrem šířky a výšky. Mezi hlavní cíle patřilo prozkoumání režimu proudění pomocí různých metod včetně použití sondy se žhaveným filmem, dále prozkoumání vlivu dvou typů drsností stěn kanálku a objasnění některých jevů spojených s aerodynamickým ucpáním vlivem tření. Kromě samotného popisu a rozborů experimentu práce obsahuje také detailní popis kalibrace sondy se žhaveným filmem a doprovodných numerických výpočtů.

Bylo pozorováno, že i při značném poměru délky a výšky kanálku, který se pohyboval v rozmezí 50 až 200, bylo proudění ve většině měřených režimů, kromě případu s výškou kanálku $h = 0.5\,\mathrm{mm}$, přechodové. Efekt různě drsných stěn byl zkoumán pomocí kvalitativních i kvantitativních měření pomocí sondy se žhaveným filmem, přičemž kvantitativní měření poskytlo data o smykovém tření v pěti bodech podél kanálku pro dva vybrané režimy proudění. Další analýzy prokázaly, že ve zkoumaných kanálech není možné použít jednorozměrný model proudění pro věrohodné určení smykového tření. Teoretické rozbory a numerické simulace ukázaly, že k aerodynmickému ucpání dochází vlivem ztrát při nižším protitlaku, než odpovídá ideálnímu případu. Výsledky těchto rozborů a z nich odvozených vztahů jsou přehledně zobrazeny do grafů.

Klíčová slova

úzké kanály, minikanál, stlačitelné proudění, smykové napětí, žhavený film

Table of Contents

Nomenclature

Non-dimensional Numbers

M	Mach number	1
Re	Reynolds number	1

Greek Symbols

δ^*	displacement thickness	m
η	thermodynamic efficiency	1
γ	ratio of specific heats; intermittency	1
ν	kinematic viscosity	$\mathrm{m}^2 \cdot s^{-1}$
ω	specific turbulence dissipation	s^{-1}
π	pressure ratio (ratio of the back pressure (settling chamber pressure) to inlet total pressure)	1
ρ	density	$\mathrm{kg} \cdot \mathrm{m}^{-3}$
τ_w	wall shear stress	$\mathrm{N} \cdot \mathrm{m}^{-2}$
φ	exit pressure ratio (exit plane pressure to inlet total pressure)	1
ζ	total pressure loss coefficient (equation (6))	1

General Symbols

C_1	hot-film sensor calibration constant	$\mathrm{V}^2 \cdot \mathrm{K}^{-1}$
C_2	hot-film sensor calibration constant	m
c_p	specific heat capacity at constant pressure	$\mathrm{J} \cdot \mathrm{kg}^{-1} \cdot \mathrm{K}^{-1}$
h	channel height	m
h_f	fence probe height	m
k	turbulent kinetic energy	$\mathrm{m}^2 \cdot \mathrm{s}^{-2}$
$\dot{m}$	mass flow rate	$\mathrm{kg} \cdot \mathrm{s}^{-1}$
p	pressure	$\mathrm{N} \cdot \mathrm{m}^{-2}$
R	specific gas constant	$\mathrm{J} \cdot \mathrm{K}^{-1} \cdot \mathrm{kg}^{-1}$
s	specific entropy	$\mathrm{J} \cdot \mathrm{K}^{-1} \cdot \mathrm{kg}^{-1}$
T	thermodynamic temperature	K
Tu	turbulence intensity	%
u	mean flow velocity	$\mathrm{m} \cdot \mathrm{s}^{-1}$
u_*	shear velocity, defined as $u_* = \sqrt{\frac{\tau_w}{\rho}}$	$\mathrm{m} \cdot \mathrm{s}^{-1}$
V	electrical voltage	V
x	length coordinate	m
y	wall distance	m
y^+	dimensionless wall-normal distance $y^+ = \frac{y u_*}{\nu}$	1

Subscripts

$*$	critical conditions
0	stagnation conditions, zero flow conditions
e	related to channel exit plane
∞	ambient conditions
s	property of sensor
son.	sonic conditions ($M = 1$)

1 Introduction

Due to its engineering importance, the flow in pipes and channels has been studied since the dawn of the modern aerodynamics in the 18th century. The most famous people who contributed to this topic include Osborne Reynolds, Hermann Schlichting, Johann Nikuradse and Lewis Ferry Moody. In 1944, the latter put available experimental data to one single diagram forming the well known *Moody Chart* which relates the Darcy friction factor to Reynolds number Re for various relative roughness of the surface. The Moody chart and all empirical rules upon which it is based are still widely used in engineering practice. However, these empirical rules are mostly based upon following assumptions

- The fluid flow is incompressible.
- The flow occurs in pipes of circular cross-section.
- The flow is fully developed.
- The surface is either aerodynamically smooth or the surface roughness is treated using equivalent sand grain roughness.

This makes such relations barely applicable to many engineering applications which does not meet some of the mentioned assumptions. One of such flows which requires deeper exploration is the flow of compressible fluid in relatively narrow channels. This kind of geometry frequently appears in screw-type compressors, control valves and labyrinth seals of steam turbines or in a gap between an impeller and a case in radial turbines and compressors. This thesis aims to experimentally and numerically examine the flow of a compressible fluid in a simple geometry of two parallel plates forming a narrow channel of the constant, rectangular cross-section, with the characteristic dimension in the order of millimetres. The knowledge and better understanding of phenomena occurring in such flow is crucial for better prediction of these flows using numerical methods which should result in more energy efficient design of mentioned machines and its components.

2 Literature Review

Most of the contemporary studies related to channel and pipe flow are devoted either to study of the physical mechanism of the transition to turbulence or to the flow in heat exchangers. In the first case, the research is usually concentrated on the flow of incompressible fluid in aerodynamically smooth pipes. The fluid velocities are rather low to obtain $Re \approx 2\,000$ and also to enable the usage of sensitive techniques of flow visualisation and measurements. The aim is usually to study the flow stability, critical conditions influencing the transition from laminar flow to turbulent and phenomenon of relaminarization [1][2]. In the second case of heat exchangers, the research mostly focuses on the increase of its efficiency [3]. In recent decades, a focus is also on microfluidics and nanofluidics, which deal with channels with the characteristic dimensions in the order of micrometres and nanometres respectively.

This work follows upon a previous research done in the Department of Fluid Dynamics of the Institute of Thermomechanics of the Czech Academy of Sciences [4][5] and upon a previous work of the author conducted in the recent years therein [A1][A2][A3]. The previous research

was motivated by the need to explore the flow in clearance gap in a dry screw compressor. The dimension of the clearance gap throat in the tested type was ranging from 200 μm to 500 μm which belongs to the category of microchannels. Numerical simulations and qualitative experimental study using Schlieren methods were carried out resulting in successful validation of the analytical model represented by Oseen equation [5]. Further research was focused on constant cross-sectional area channels with the characteristic dimension in the order of millimetres [4]. The aim of the later research was to experimentally investigate the flow of compressible fluid in channels of the height ranging from 0.5 mm to 2 mm, length of 100 mm and 200 mm, and of various width. The study revealed almost non-existing secondary flow structures, such as corner vortices, typical for rectangular channels of the standard size. The extent of secondary flow structures depends significantly on the channel aspect ratio (channel width to height), which was ranging from 5 to 200. The authors also aimed to investigate the losses and friction factor. For the determination of the friction factor, they used the method based on the one-dimensional model of an adiabatic flow with friction (Fanno flow) described for example in [6]. This method is based on the evaluation of the friction factor from the known distribution of the Mach number along the channel. However, in the case of aerodynamically choked flow, this method yields zero value of the mean friction factor in the vicinity of the channel exit plane. Since the exit plane is a location where the maximal value of the entropy is reached, it would be strange if the value of the friction factor was approaching zero in this location. Authors conclude with the suggestion to pay more attention to flow structures and the value of the friction factor in the vicinity of the exit plane and urge for the use of other methods of the wall shear stress measurements. Possibly the methods which would not rely solely on pressure measurements.

Further research included repeated measurements and numerical simulations of the similar geometry - channel formed by two parallel plates of the length and width of 100 mm with a variable height from 0.5 mm to 4 mm [A1],[A2]. The aim was to obtain data using pressure and optical methods and explore the possibility of CFD simulations. The measured data were also used for the validation of the in-house code developed at the Faculty of Applied Sciences of the University of West Bohemia in Pilsen and for the calibration of RANS turbulence models [7]. Subsequent work was focused mostly on the improvement of the measurement facility and modelling using the developing code based on Discontinuous-Galerkin finite element method [A3] [8].

The problem of choked flow with losses is addressed e.g. in theoretical study of Hyhlík et al. [9] and in numerical and experimental investigation of Lijo et al. [10]. The work of Lijo deals with the flow in circular pipes and explore the influence of the losses on the critical conditions with the motivation to investigate this phenomenon influencing performance of sonic nozzles of the small diameter, which are used as a standard flow meters. Lijo concludes that the friction losses, and thus the presence of relatively thick boundary layer (inner pipe diameter was 15 mm), affect the choking in such a way that the sonic line is shifted from the exit plane upstream. And this shift depends, according to them, strongly upon the driving back pressure ratio. They also found out that the exit flow field changes even when the back pressure ratio is below the critical value of $\frac{p}{p_0} = 0.5283$ that applies for air as an ideal gas. Lijo claims that the actual critical pressure ratio, below which the further reduction of the back pressure does not influence the flow in pipe and the mass flow rate, is much lower than the theoretical value of 0.5283 and support this by the numerical study. The authors also address

the phenomenon of supersonic region which forms in the pipe core flow downstream the sonic line. They claim that the reason is in the thinning of the boundary layer towards the exit, possibly with a zero boundary layer thickness right at the location of an exit plane forming divergent nozzle, however, they do not give any experimental evidence of this effect.

Considerably different results were obtained in theoretical study of Hyhlík et al. [9]. In this study, the one dimensional model of the flow with friction was used to derive the theoretical relation of the critical pressure ratio (defined by the maximal value of the mass flow rate $\dot{m}$) for the constant thermodynamic efficiency η. Authors of this study derived that the critical and sonic conditions differ for any value of the thermodynamic efficiency lower then unity. Such difference would mean that the non-ideal flow would reach the maximum of the flow rate significantly before the sonic conditions occur.

It follows from the above that the flow in constant area channels of small dimensions is still deeply uncharted territory, particularly with respect to the lack of experimental data, which would allow to identify the nature of the flow and the data of the wall shear stress distribution along the channel walls. The phenomenon of the possible shift of critical conditions in the case of aerodynamically choked flow is also a topical problem awaiting deeper exploration. The aims of this work are summarized in the following section.

3 Aims of the Work

Research goals summarized in points are as follows:

- To determine what is the nature of the flow in the investigated channels using the available measurement techniques, including hot-film anemometry, and numerical simulations. And to describe the influence of the two different types of surface roughness on the flow development and possible transition to turbulence.
- To explore whether the critical conditions separates from the sonic conditions due to effects of friction under the conditions of aerodynamic choking as theoretically predicted in study [9].
- To determine whether the boundary layer might get thinner and the shear stress reduced in the region close to the channel exit.

4 Philosophy of Approach - Design of Experiments

The purpose of this section is to briefly introduce a plan how to reach the aims. The previous work on this topic revealed the necessity to choose more suitable method of surface shear stress measurement. Amongst all the conceivable methods, the hot-film anemometry was chosen since there was one *Dantec Dynamics 55R45* hot-film probe readily available. However, the disadvantage of this method is its tedious calibration. To tackle this, *Calibration facility* of larger dimensions was constructed, manufactured, and used for the calibration against the fence probe. Later, with the already calibrated hot film probe, the measurements were to be conducted in narrow channels using *Narrow channel facility*.

Thanks to the cooperation with *PBS Velká Bíteš a.s.* company, which tackled the problem of flow in the gap between radial turbine impeller and the casing with an impact on the

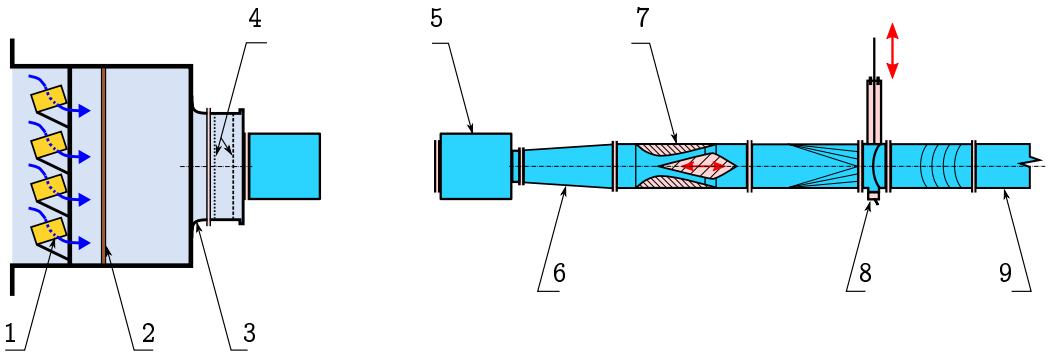

Figure 1: Schematic diagram of the modular in-draft type wind tunnel: 1-Silica gel drier, 2-Filters, 3-Bellmouth contraction, 4-Honeycomb and wire meshes, 5-Settling chamber, 6-Diffuser, 7-Controll nozzle, 8-Quick acting valve, 9-Main duct to vacuum tank.

ventilation of this gap and subsequently the cooling of the impeller, we obtained precisely manufactured channel walls with three types of surface finishing. Therefore, we were able to extend the research by the exploration of the influence of surface roughness. As the measurement in the confined area is difficult and not always possible due to its small dimensions, the numerical simulations are also an essential part of this work, in particular with regard to the phenomenon of aerodynamic choking and possible shift of critical and sonic conditions.

The chosen combination of measurement methods should provide novel data, the later analysis of which together with the results of numerical simulations will help to answer the questions outlined above.

5 Experimental Facilities & Measurement Techniques

5.1 Introduction

The experimental part of this work was carried out in the Laboratory of internal flows of the Institute of Thermomechanics of the Czech Academy of Sciences in Nový Knín. The laboratory is equipped with a modular in-draft type wind tunnel facility (Figure 1). The settling chamber enables to mount different models or test sections to be measured using various techniques such as pneumatic methods, optical measurement techniques using Mach-Zehnder interferometer and hot-film/hot wire anemometry. The in-drafted medium might be either non-preconditioned air sucked directly from the laboratory or dried and filtered outside ambient air. The control nozzle enables to continually change the pressure in the settling chamber from approximately 0.01 MPa up to the value close to the ambient atmospheric pressure. The techniques and devices used for the present investigation are briefly introduced in the following paragraphs.

5.2 Narrow Channel Facility

The narrow channel facility is shown in Figure 2. The actual channel is formed by two parallel walls made of stainless steel with optical windows as the side walls allowing optical access. The upper and lower wall is attached to the adjustable supporting elements, which enable adjusting the gap between the walls in the range from zero to approximately 4 mm. The inlet part is of the quarter-cylinder shape of 8 mm in radius and the following straight part of the

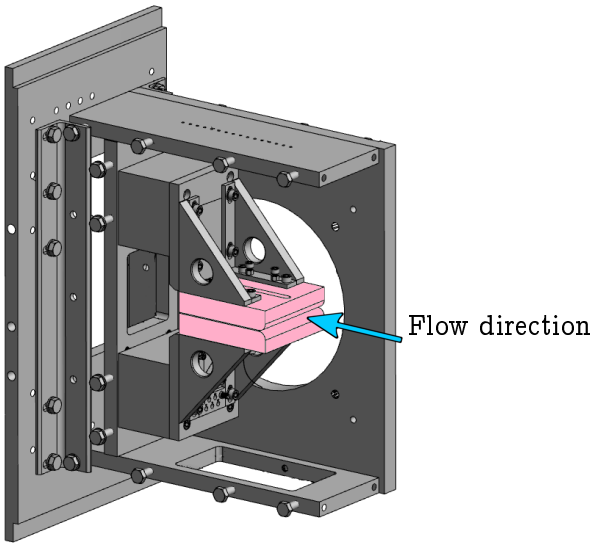

Figure 2: *View on the 3D CAD assembly of the narrow channel facility with uncovered left side wall and with the plates forming narrow channel coloured in purple.*

channel is 100 mm long and the width of the channel is 100 mm. The whole assembly of the channel consisting of steel plates, supporting elements, and optical windows is fitted in the casing which is connected to the settling chamber (No. 5 in Figure 1).

As the surface roughness effects were of particular interest, the channel walls were manufactured with three different surface finishes of the channel straight part. One pair of the walls was smooth and two others were roughened by end-milling process with the different lay of a surface (the direction of predominant surface pattern). One pair has the lay of the surface perpendicular to the flow direction (cross-flow) while the other has it in the direction of the flow (streamwise).

5.3 Hot-Film Sensor Calibration Facility

With regard to the geometry of narrow channels, it was decided to perform the calibration of the hot-film sensor in a geometrically similar device, yet of the dimensions large enough to enable measurements using other more intrusive techniques such as Preston or Stanton tubes or sublayer fence probes. Aforementioned considerations led to a design and manufacture of the facility hereafter referred to as *Calibration Channel*. The calibration channel, pictured in Figure 3, has an inlet of Bernoulli lemniscate shape. The follow-up 1.526 m long straight section of constant cross-sectional area is of the cross-sectional dimensions of 200x10 mm. The whole internal surface of the channel and inlet are smooth-finished and the transitions from the inlet part to the straight section were puttied and sanded smooth. The facility was adapted for the measurements using numerous techniques such as pitot probe, sublayer fence probe, hot-wire probe or surface hot-film sensor.

5.4 Pneumatic Measurements

Besides the measurements of the static pressure distributions along the calibration channel, the measurements of the total pressure in the channel axis using Pitot probe were also performed together with the measurements of total pressure profiles in a few strategic locations

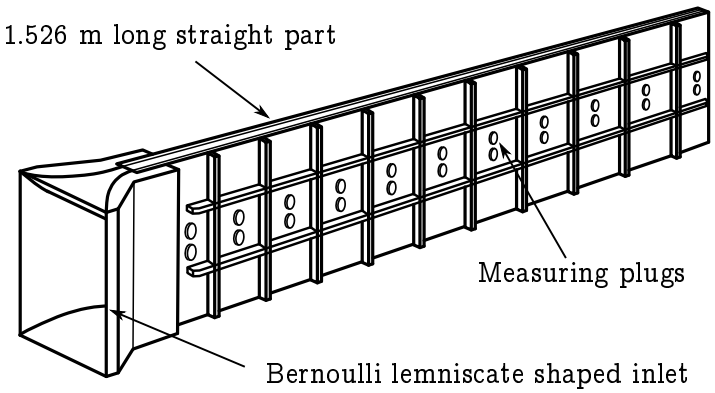

Figure 3: *Schematic depiction of the calibration channel.*

to assess the development of the flow along the channel. Measurements of the profiles of the total pressure in the calibration channel were conducted using the traversing device, incorporating calibrated micrometric screw enabling precision positioning of the Pitot probe within the channel. The total pressure data were corrected for wall proximity effects according to MacMillan [11].

For the narrow channel facility, the static pressure distribution was also measured, however, due to small dimensions the total pressure was measured close to the exit plane only (approximately 2 mm upstream the exit plane). In all measurements both the pressure at the inlet p_{in} and the pressure in the settling chamber p_{b} were also measured.

For the pressure data acquisition, two 16 channel *PSI 9116* pressure scanners and *Texas Instruments* data acquisition module connected to PC were used. Each scanner integrates 16 silicon piezoresistive pressure sensors and microprocessor that performs a correction for sensor zero, span, linearity, and thermal errors. The manufacturer guarantees the system accuracy of up to $\pm 0.05\%$ of the full-scale reading which is 15 PSI (103.4 kPa) [12]. The connection between the pressure scanners and pressure taps was realised through the sealed tubing of 0.5 mm in diameter.

5.5 Optical Measurements

Laboratory of internal flows in Nový Knín is equipped with a unique Mach-Zehnder type interferometer. The optical measurements were conducted in an *Infinite-Fringe* set-up. During the measurement there are significant density gradients and thus gradients of the index of refraction in the test section, causing the phase shift of the sample beam. If there is a phase shift between the sample and reference beams, the interference patterns are formed and it is possible to take the interferograms using the digital camera. The camera used was 80 Mpx *Phase One XF IQ3*.

5.6 Sublayer Fence Probe Measurements

The working principle of the sublayer fence probe is similar to that of Preston or Stanton probes and is based upon the assumption of the self-similar velocity distribution in the turbulent boundary layer known as *Law of the Wall*. The law of the wall states that in the turbulent boundary layer, there is a region close to the wall where the velocity profile depends upon the wall shear stress, physical properties of the fluid, and the distance from the wall and at the

same time does not depend on the state of the flow outside the boundary layer. This law is usually given in the form

$$\frac{u}{u_*} = f\left(\frac{yu_*}{\nu}\right), \tag{1}$$

where $u_* = \sqrt{\frac{\tau_w}{\rho}}$ is the friction velocity and $\frac{yu_*}{\nu} = y^+$ is the dimensionless wall distance.

The law of the wall thus enables us to determine the wall shear stress from the velocity measured in the region of its applicability and if the physical properties of the flow are known. If the obstacle in the form of fence is placed in the law of the wall region, then the following relation between fence height h_f, pressure difference measured using pressure taps located immediately upstream and downstream of the fence Δp, and shear stress can be written:

$$\frac{\Delta p}{\tau_w} = f\left(\frac{h_f u_*}{\nu}\right). \tag{2}$$

Assuming the universal validity of the law of the wall for turbulent flow, the above outlined relations are also universal and the obtained calibrations can be used for any geometrically similar probes [13].

5.7 Surface Hot-Film Sensor Measurements

Though the idea of relating the heat transfer from an electrically heated strip embedded in a surface and the wall shear stress is known for several decades (e.g. pioneering work of Liepmann and Skinner [14]), its usage for quantitative measurements is still limited due to difficult calibration. The difficulty lays mainly in the heat transfer to the probe substrate, which is problematic to quantify, and the dependency on the flow temperature, both of which must be compensated.

Despite all the drawbacks, the method of wall hot-film measurement is important since it is one of the few minimal intrusive methods suitable to effectively investigate the surface shear stress even in small confined geometries where the complete measurement of boundary layer is impossible. Among its significant benefits, we can also include fast frequency response and thus the ability to provide time-resolved data, from which it is possible to identify boundary layer transition and flow separation even using uncalibrated sensor [15].

The calibration of a surface hot-film sensor might be made against a Preston tube, for which the universal calibration was developed (assuming the flow with the known law of the wall across the tube diameter), or against a calibrated Stanton tube or sublayer fence probe. Due to the availability of a calibrated sublayer fence probe and due to its better sensitivity (almost double the pressure difference Δp than in the case of a Stanton probe), the latter option was chosen. The calibration procedure and measurements are described in detail in section 7.

5.7.1 Flow Character Identification

One of the advantage of the hot film-probe is its capability of high-frequency sampling of the flow instabilities. This feature can be advantageously used for the flow characterization from the sensor raw signal without the necessity of sensor calibration. Several methods have been devised and reported to interpret the flow regime from a raw hot-film probe signal [16][17].

These methods are most commonly based on the change of the signal root mean square (RMS) or other signal characteristics such as the signal skewness. The one reported by Hodson et al. [16], which uses skew function, had already been used before in Laboratory of internal flows of the Institute of Thermomechanics for qualitative evaluation of the hot-film array measurements of the flow past a transonic airfoil [A4]. This method uses the skew function (SF) defined as

$$SF = \frac{\frac{1}{n}\sum_{i=1}^{n}(x_i - \overline{x})^3}{\left[\frac{1}{n-1}\sum_{i=1}^{n}(x_i - \overline{x})^2\right]^{\frac{3}{2}}}, \tag{3}$$

where x stands for measured signal variable (voltage) and $\bar{x}$ its mean value. According to this method a typical nature or bypass transition behaviour in terms of intermittency γ, which describes the fraction of time during which the flow at a certain position is turbulent, might be identified [17]. Zero skewness corresponds to the flat time-resolved signal without any random disturbances (e.g. pure laminar flow, $\gamma = 0$; or pure turbulent flow, $\gamma = 1$). For $\gamma = 0.25$, the skewness reaches its maximum. At $\gamma = 0.5$ where equal periods of laminar and turbulent flow exist, the skew function decreases to zero. This point at the same time typically coincides with the random fluctuation maximum. At $\gamma = 0.75$ the skewness exhibits a minimum. The shortcoming of this method is that the signal noise and other random effects (e.g. shock oscillations) may lead to a noisy and messy skew distribution which might then deviates significantly from the described ideal distribution. However, this concerns in particular the flows past cascades where shock waves appear frequently, which is fortunately not so much the case of the channel flow.

6 Numerical Simulations

6.1 Introduction

For its cost effectiveness and the ability to explore many design variants in relatively short time, the numerical simulations play increasingly important role in nowadays applied research and industry. Since its first practical usage in the 1960s, the Computational Fluid Dynamics (CFD) established itself not only as a powerful design tool but in many cases represents a role of theory, to which the results of experiments are compared. Nevertheless, one might keep in mind that the mathematical models are limited by assumptions from which the models were derived. For that reason, it is broadly accepted that the numerical simulations should be accompanied by validation experiments. Although this is true, it is useful to accompany also an experimental research with CFD computations, which in this case might provide additional data and lead to better understanding of the given problem. In this work, the CFD is used both as a tool to support the experiments and as a subject of investigation. Though, in the case of *calibration channel* the simulations were used to support the experimental results, while in the case of the narrow channel flow, the most appropriate numerical model was searched for. Besides that, the results of both experiments were also used for a validation purposes of the numerical solver based on the discontinuous Galerkin method developed at the Research centre of the Faculty of Applied Sciences (NTIS) at the university of West Bohemia.

6.2 Numerical Methods

The numerical computations presented in this thesis were performed using Ansys Fluent 19.3 commercial code. This software package uses finite volume method to solve the governing Navier-Stokes equations for compressible fluid flow. Since the air could be considered as an ideal gas for the conditions considered in the narrow channels, the ideal gas flow model was used throughout all computations.

For the turbulence modeling the Reynolds-averaged Navier-Stokes (RANS) approach was chosen. Throughout this work, various RANS turbulence models were used either to support the calibration measurements for the hot-film and sublayer fence probes in the case of calibration channel or to obtain computational data of the flow in narrow channel. Simulations of the calibration channel were performed using the k $-\omega$ SST and EARSM $-\omega$ fully turbulent models and using SST – Transitional model capable to predict the transition to turbulence. However, the usage of the transitional models for the simulations of the calibration channel was later abandoned due to the use of the turbulators at the channel inlet, which makes the simulation of the transition unimportant since the turbulent regime was forced from the very inlet of the channel. In the case of the narrow channels, the SST – Transitional and k $-\omega$ SST turbulence model with the intermittency model of transition were used besides the already mentioned k $-\omega$ SST and EARSM $-\omega$ turbulence models.

All computations were performed using the density based implicit solver and using the second order accuracy upwind schemes in space. The inviscid fluxes were approximated using the Advection Upstream Splitting Method (AUSM) upwind scheme with linear reconstruction.

The grid convergence study using two finer meshes was performed according to the methodology described by Roache in [18] resulting in Grid Convergence Index of approximately 0.3 % for coarse meshes, which is well acceptable.

7 Hot-Film Sensor Calibration Procedure

After several attempts the semi-empirical calibration method of Davies described in [19] was chosen as the most suitable one for the use in our investigation. This method is based on the continuous measurement until the temperature equilibrium is reached, which took approximately 20 minutes in our case, and on the subsequent measurement immediately after switching off the airflow giving zero flow voltage V_0. Using the zero flow voltage, the temperature variation effects can be successfully eliminated for thermal equilibrium flows. The relation for the wall shear stress is then given by equation

$$\tau_w = \left[\frac{V^2 - V_0^2}{C_1(T_s - T_\infty)}\right]^3 + C_2\frac{\mathrm{d}p}{\mathrm{d}x}, \tag{4}$$

where C_1 and C_2 are calibration constants, incorporating the physical properties of the fluid and the dimensions of the sensor. To obtain the calibration constants, the set of measurements in the calibration facility using the sublayer fence probe and hot-film sensor was carried out. The obtained data were used for the determination of the calibration constants using optimization script written in MATLAB programming environment.

7.1 Hot-Film Probe Calibration Measurements

For the calibration measurements, the same driving pressure ratios of the settling chamber pressure to inlet pressure $\pi = \frac{p_b}{p_{01}} = 0.3$; 0.6 and 0.8 were chosen. Such range of pressure ratios should cover sufficiently large range of the wall shear stress values in the calibration channel. For each of these pressure ratios, the values of the wall shear stress were measured along the channel axis using the sublayer fence probe together with the distribution of the static pressure. Then, the measurements were conducted operating the hot-film probe in the calibration channel for the same regimes given by the driving pressure ratios, and thus, the same wall shear stress distributions, which enabled us to determine the link between the voltage across the hot-film sensor V and the aerodynamic wall shear stress τ_w using the semi-empirical calibration method of Davies.

To obtain the calibration constants C_1 and C_2 for the relation (4), the optimisation algorithm based on the minimization of an objective function was written in MATLAB. The *objective function* was of the following form

$$f(V,\, V_0,\, p,\, T_s,\, T_\infty) = \sqrt{\left\{ \left[\frac{V^2 - V_0^2}{C_1 (T_s - T_\infty)} \right]^3 + C_2 \frac{\mathrm{d}p}{\mathrm{d}x} - \tau_{w\,\mathrm{Fence}} \right\}^2}. \tag{5}$$

The optimization algorithm (Nelder-Mead simplex direct search) then searched for the combination of the calibration constants so as the objective function is minimized in the least squares sense for the given test data consisting of the vector of wall shear stress measured by the sublayer fence probe and the corresponding vector of the voltage $V^2 - V_0^2$, where V is the voltage measured on the hot-film sensor after the temperature equilibrium was reached for a given flow regime and V_0 is the sensor voltage measured immediately after the switching off the flow. It should be noted that such calibration can only be used for the same sensor operated under the same overheat temperature in the air and if the sensor is mounted in the material of the same thermal conductivity as was used during the calibration.

8 Narrow Channel Measurements

To effectively tackle the defined objectives, the narrow channel measurements were conducted in three stages. During the first stage, the optical measurements of the channel of the heigh of 2 mm was carried out for several pressure ratios and for each of three surface finishes. Other channel heights were not measured in this stage due to limitation of the optical method, which requires sufficient channel height to prevent light reflections from channel walls that make measurements impossible. These measurements are continuing of the previous investigation conducted in Nový Knín laboratory [A5][A2][A6][A3], but now improved by the use of the new high resolution camera and improved construction of narrow channel facility providing higher accuracy of the channel height setting.

The second stage comprises of measurements of all surface roughness variants in channels of the height of 0.5; 1 and 2 mm. Each of these combinations were measured for pressure ratios 0.3; 0.6 and 0.8. Since the number of measured regimes was too large for time demanding quantitative measurements using hot-film probe, the regimes were first investigated qualitatively without the need for long continuous measurement runs necessary to achieve

temperature equilibrium. Besides that, the pneumatic measurements using static pressure taps and the measurements of the total pressure were carried out during this stage.

The third stage included quantitative measurement using the hot film probe at the regimes chosen based on the interim analysis of the first stage measurements. This stage was primarily intended to measure shear stress in the channel and its near exit region and to complete measurements from the stage two.

9 Results & Discussion

9.1 Flow analysis

As concluded in the introductory section, the problem of identifying whether the flow in narrow channels of dimensions comparable with the investigated channels is laminar or turbulent is still a topical problem of fluid dynamics. This section provides analysis of numerical simulations and of measured data including data obtained using the hot-film probe with the aims to shed more light on the nature of the flow in the narrow channels.

9.1.1 Results of the Pneumatic Measurements

The first available and easiest to process data were those measured using pneumatic methods, therefore, its analysis and comparison with the numerical simulations were also conducted first, resulting in following findings.

Graphs in Figures 4a, 4b and 4c show the comparison of computed and measured distributions of the static pressure (normalized by the inlet total pressure p_{01}) along the channel for three channel heights and three different pressure ratios. It is apparent that closer to the channel inlet, the measured distributions falls approximately in between distributions computed using fully turbulent and transitional models. However, with increasing x-coordinate, the fully turbulent models seem to perform better, while there is almost no difference between k $-\omega$ SST and EARSM-ω models in cases for which both these models were tested. Later on, the pneumatic measurements were completed with the measurements on the channels equipped with rough walls. It was observed that the cross-flow roughness shifts the distribution upwards with respect to the smooth wall. This difference is most apparent for the moderate pressure ratio $\pi = 0.6$ and increases towards the channel exit. The streamwise roughness on the other hand shifts the distributions lower with respect to the smooth wall case. This is most likely caused by increase of the effective cross-section of the channel, resulting in distributions which correspond to larger channel height than the nominal height measured using filler gauges. This effect apparently weakens as the ratio between the roughness and the channel height became smaller with increasing channel height, which results in almost no difference between the smooth wall and streamwise roughness in the case of the channel height $h = 2\,\mathrm{mm}$.

Another comparison provides the graph in Figure 5. This graph shows values of total pressure measured in the mid channel in location $x = 98\,\mathrm{mm}$ (2 mm upstream the exit plane) with respect to pressure ratio π for various channel heights and compares it to computed values. The comparison reveals that both transitional models (Transitional SST and k $-\omega$ SST with the intermittency model of transition) significantly over-predicts the entrance length resulting

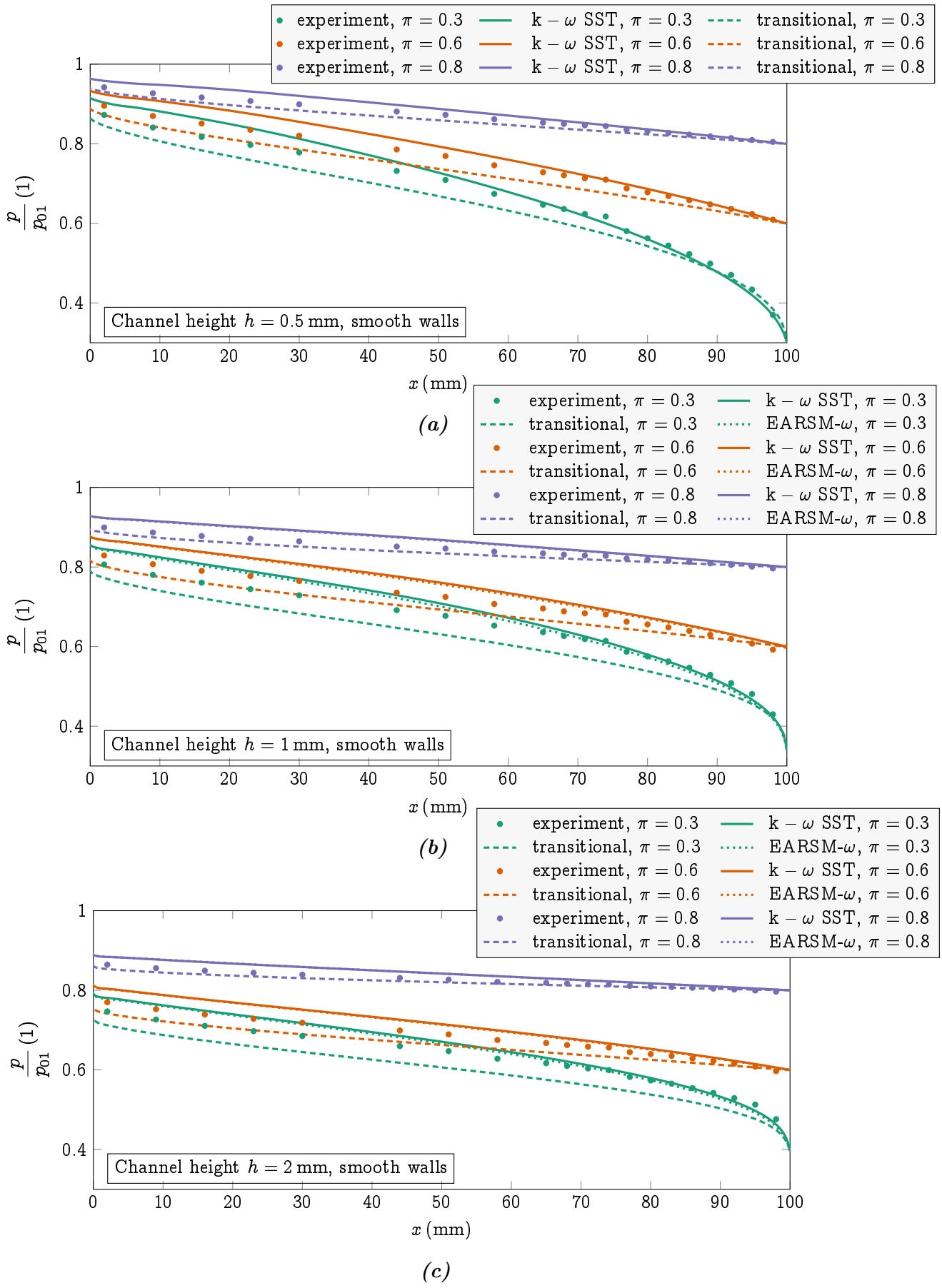

Figure 4: *Distributions of the normalized static pressure* $\frac{p}{p_{01}}$ *along the channel length for channel of the height* $h = 0.5\,\text{mm}$ *(a),* $h = 1\,\text{mm}$ *(b) and* $h = 2\,\text{mm}$ *(c) each for pressure ratios* $\pi = 0.3$, 0.6 *and* 0.8. *Comparison of measurements and simulations.*

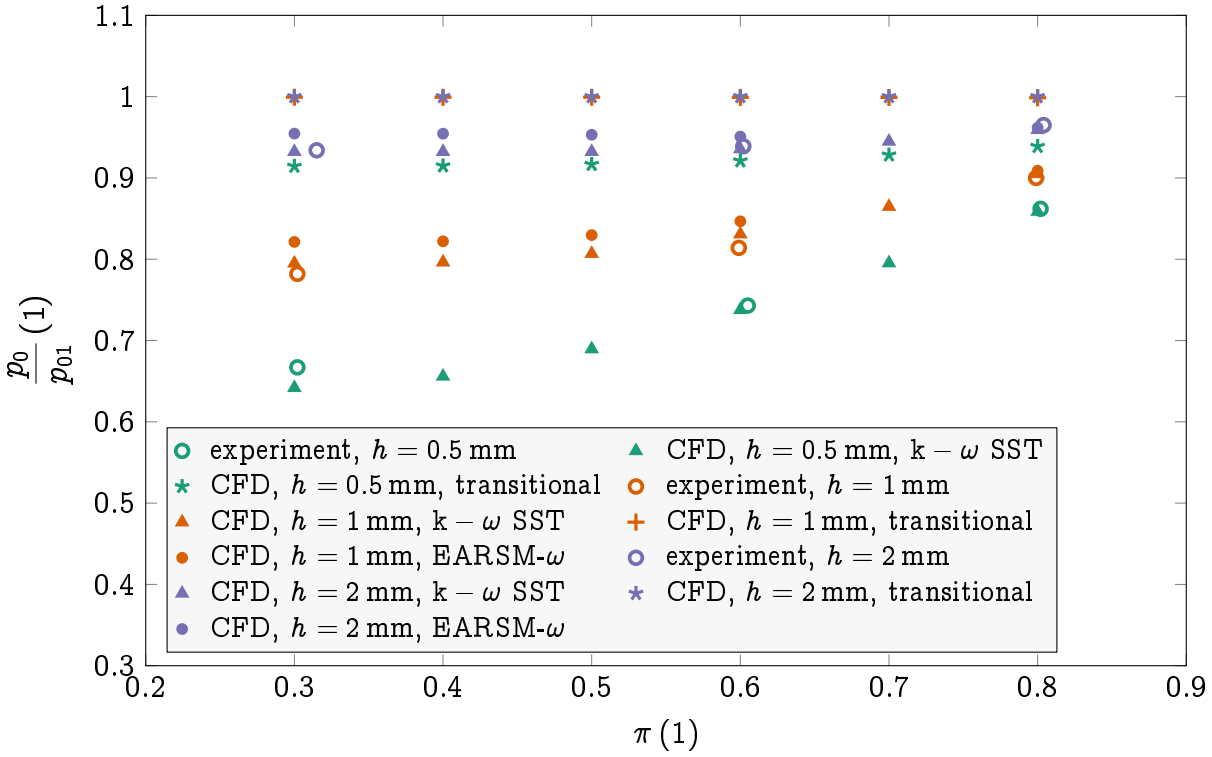

Figure 5: *Normalized total pressure* $\frac{p_0}{p_{01}}$ *measured in mid channel in location* $x = 98$ mm *with respect to pressure ratio* π *for various channel heights* h.

in almost no total pressure drop along the entire channel length. This is most apparent for channel heights $h = 1$ and $h = 2$ mm. In the case of $h = 0.5$ mm, the computed total pressure drop is present but its magnitude is still much lower then the measured one.

When the measurements were completed with rough wall measurements, the total pressure loss was evaluated in terms of total pressure loss coefficient

$$\zeta = 1 - \frac{p_0}{p_{01}}. \tag{6}$$

These results are summarized in the graph in Figure 6, showing the total pressure loss coefficient ζ plotted against the pressure ratio π for various channel heights and roughness. It is rather surprising that the higher pressure loss was measured for smooth variants of the channel walls than for its rough variants. This is most apparent for the channel height $h = 2$ mm. The plot pictures also the error bars which show standard deviation of both total pressure loss coefficient ζ and pressure ratio π. It is well apparent that smooth wall variants exhibits for most cases larger deviations most likely due to stronger flow oscillations, nevertheless, this hypothesis needs to be explored by further measurements.

Even though the measuring facility underwent major improvements compared to the version used before [A5] and total pressure data gave new valuable results, it is still difficult to assess the mode of the flow and its development based on the pneumatic measurements only. Yet, having such data is important not only for assessments of the numerical simulations but besides that also for further investigation since the knowledge of pressure distributions is essential for wall shear stress evaluation using a hot film probe.

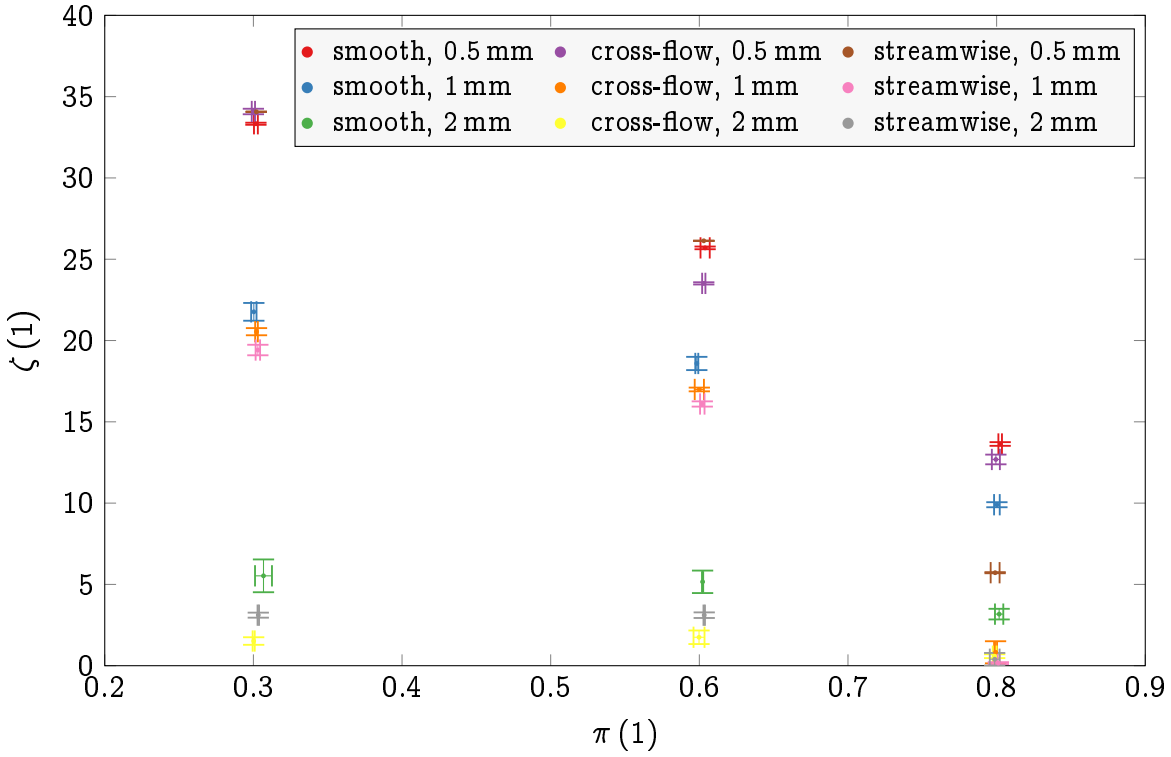

Figure 6: *Total pressure loss coefficient ζ (6) plotted against the pressure ratio π for various channel heights and wall roughness.*

9.1.2 Results of the Optical Measurements

As a next step, the assessment of the optical measurements and its comparison with computed flow fields was made. Although the new high resolution camera was used for the optical measurements a substantial part of the flow field in the wall vicinity is not clearly visible perhaps due to shadow caused by not ideal alignment of the optical path with the channel walls. Therefore, it is not possible to evaluate density profiles up to channel walls to estimate wall shear stress. Nevertheless, at least some qualitative assessment of the measured flow fields to computational results is possible.

Figure 7 shows the computed density contours obtained using k $-$ ω SST turbulence model (top of each subfigure) and interferograms of the exit region for channel height $h = 2$ mm and three different pressure ratios. As can be seen, both the shape of the density contours close to the channel exit and flow structures downstream the sudden expansion seem to show quite a good agreement with the interferograms. This might lead to a conclusion that the flow in the cases above is most likely turbulent. Though, as it is impossible to evaluate the wall shear stress from the optical measurements, it is not possible to draw this conclusion with certainty. This uncertainty was later confirmed by further measurements, which revealed that the flow is not completely turbulent.

Regarding the roughened walls, the resulting interferograms are well comparable in the case of streamwise roughness, however, in the case of cross flow roughness, the interference fringes are sort of blurred. It is not clear whether it is because the light is scattered by the roughness in such way it makes the resulting image fuzzy or if it is because the flow field oscillates. To answer this question, the fast camera should have been employed but it would also require significant changes in the whole imaging system, mainly in different light source

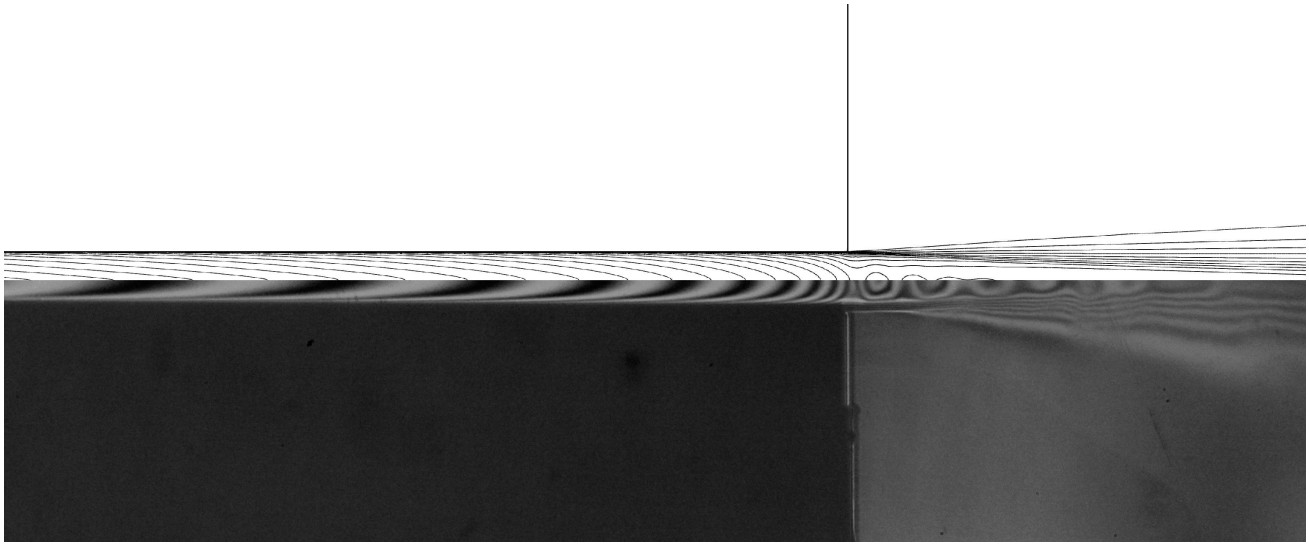

(a)

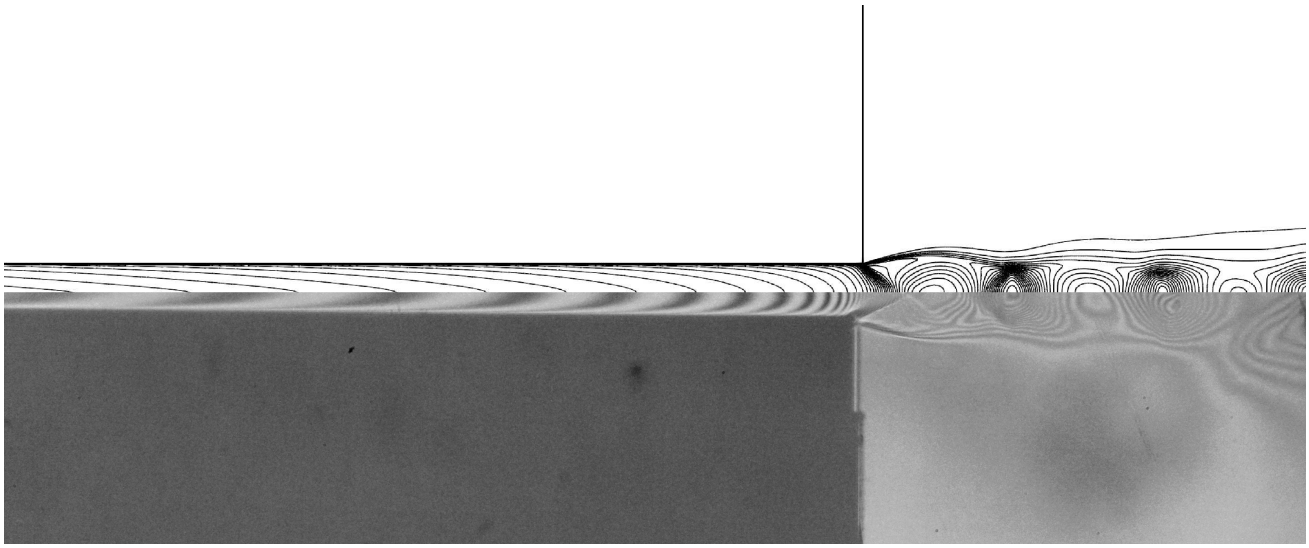

(b)

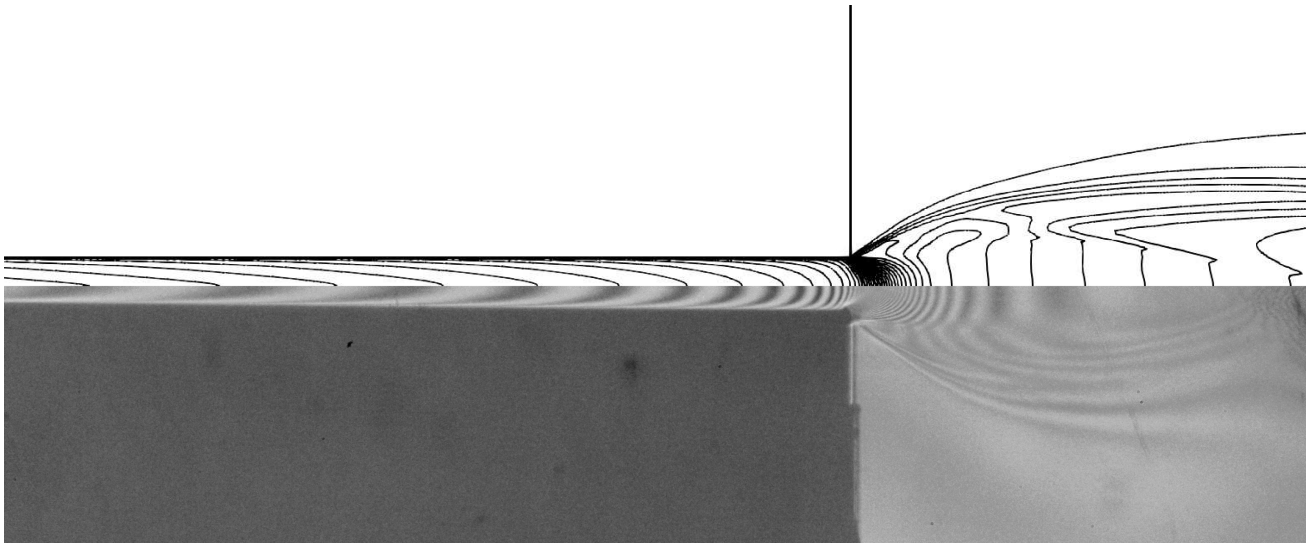

(c)

Figure 7: *Comparison of density contours computed using* $\mathrm{k}-\omega$ *SST turbulence model (top) with interferograms (bottom) for pressure ratio* $\pi = 0.44$ *(a),* $\pi = 0.219$ *(b) and* $\pi = 0.088$ *(c).*

and its synchronization with the camera. Since such an upgrade is far beyond the scope of this work, the most promising way to evaluate possible flow oscillations seams to be the hot-film probe.

9.1.3 Qualitative Hot-film Probe Investigation Results

Further insight in the problem of the flow transition in investigated narrow channels is offered by qualitative hot film probe measurements. This investigation is based on the analysis of the raw hot-film probe signal as well as the analysis based on the signal *skew function* defined by equation (3) as described in section 5.7.1.

Figures 8, 9 and 10 picture the series of graphs of the raw hot-film probe signal for smooth channel walls, three locations of the hot film probe, three different channel heights, and pressure ratio $\pi = 0.3$. It can be seen that for channel heights $h = 0.5\,\text{mm}$ and $h = 1\,\text{mm}$ the signal exhibits turbulent character from the plug No. 3, therefore, the transition in these two cases most likely completed between plugs No. 1 and 3. It is worth noting the reduced signal width in the last plug (No. 5), which is probably caused by steep expansion which occurs close to the channel exit and is more pronounced with decreasing channel height. If we look on the situation for the channel height $h = 2\,\text{mm}$ shown in Figure 10, we can see that the transition is not completed even at the location of the plug No. 5, in which the signal shows highly intermittent characteristics and the positive skew function suggests the values of intermittency $\gamma < 0.5$. In the case of increased pressure ratio, the situation is comparable with the case of the pressure ratio $\pi = 0.3$ without any major qualitative differences observable in the raw signal.

The situation become different in the case of rough walls. In the channel of the height $h = 0.5\,\text{mm}$ and cross-flow roughness, the significant oscillations, which show nearly harmonic behaviour in the plug No. 1, appeared in the signal. Using the spectral analysis, the significant frequency was identified to be approximately 590 Hz. These oscillations, however, disappeared for larger channel gaps and for increased pressure ratios π. For the channel height $h = 2\,\text{mm}$, the influence of the cross-flow roughness seems to be in shifting of the transition upstream, resulting in lower skew function value measured in the plug No. 5, which corresponds to intermittency $\gamma > 0.5$. This also explains higher standard deviations of the total pressure measured for smooth walls in the plug No. 5 as discussed earlier in Section 9.1.1. It is because in the smooth case, the fluctuation maximum related with intermittency $\gamma = 0.5$ is apparently closer to the channel exit, and thus to the plug No. 5, compared to roughened walls, in which case the fluctuation maximum occurs earlier.

Streamwise roughness appears to have very similar effect to the cross-flow roughness including shift of the transition upstream, which is, however, not so significant in this case.

9.1.4 Quantitative Hot-film Probe Investigation Results

A different point of view provides the quantitative hot-film probe investigation. Figures 11a and 11b show comparison of the computed wall shear stress distributions along the channel length with the measured data including data measured in channels with rough walls with cross-flow roughness. If we first focus on the measured data only, we can see that the smooth wall value is comparable to that of rough wall solely in the location of the first measuring plug

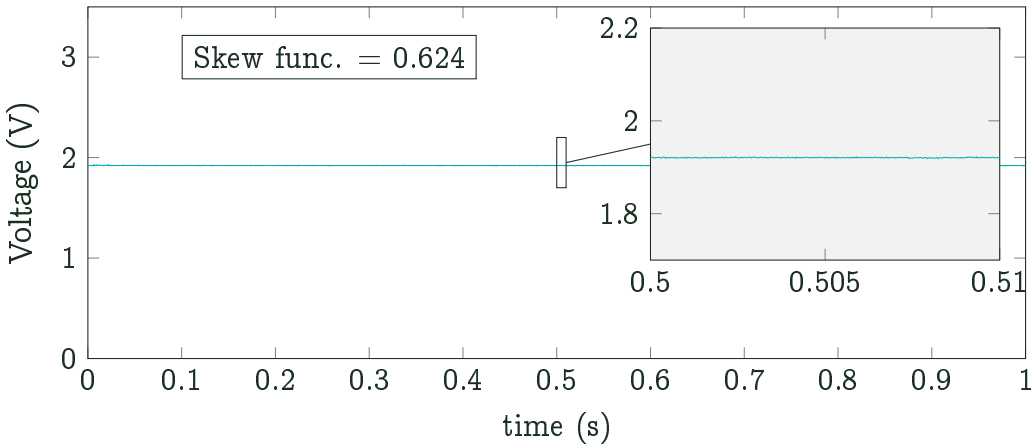

(a)

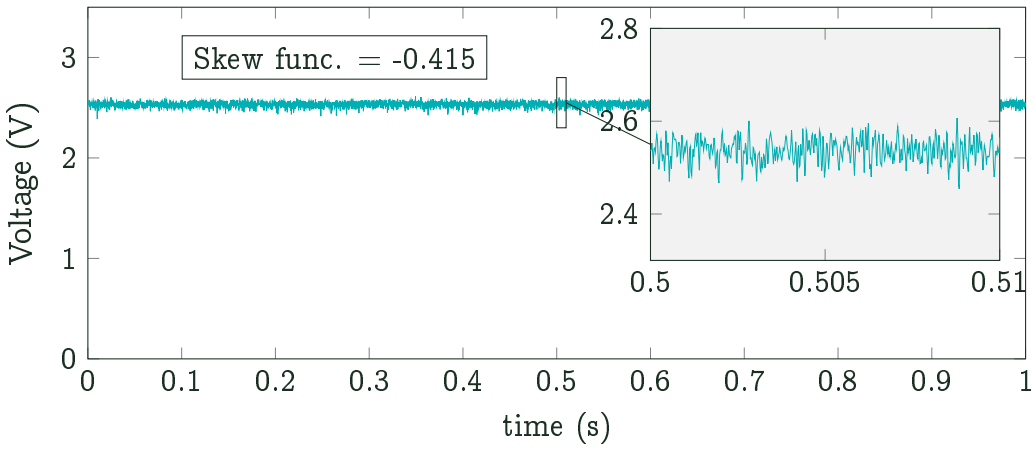

(b)

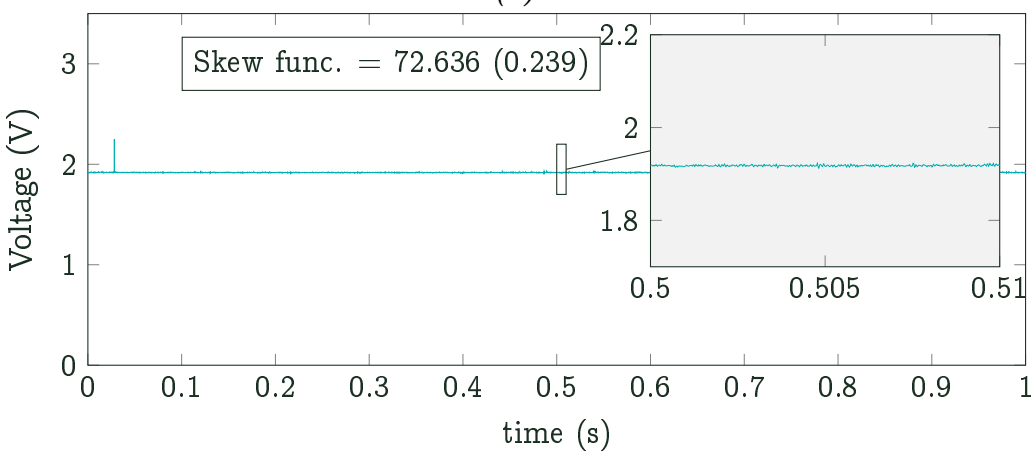

(c)

Figure 8: *Hot-film probe signal measured in plug 1 (a), 3 (b) and 5 (c) in the smooth channel of the height* $h = 0.5\,\mathrm{mm}$ *and* $\pi = 0.3$.

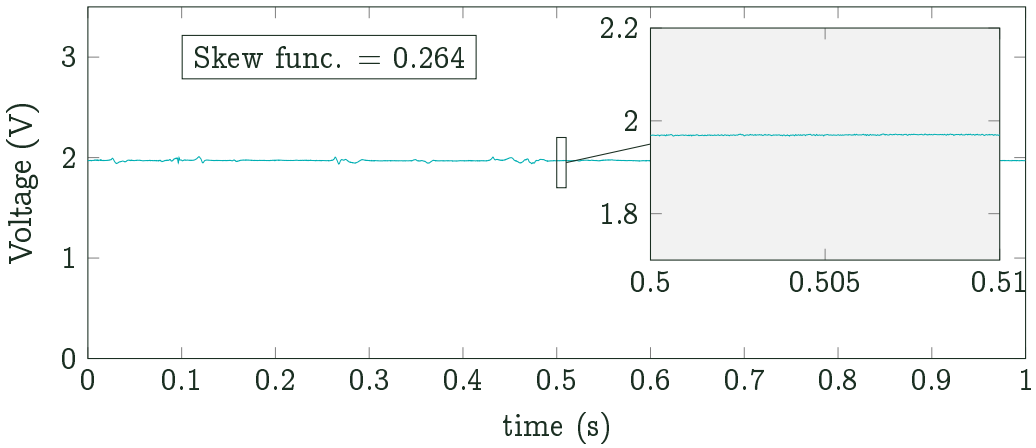

(a)

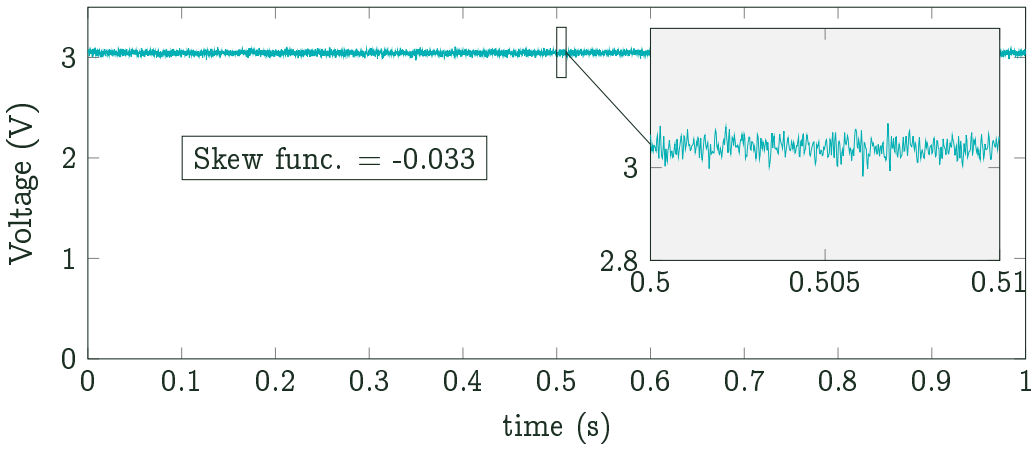

(b)

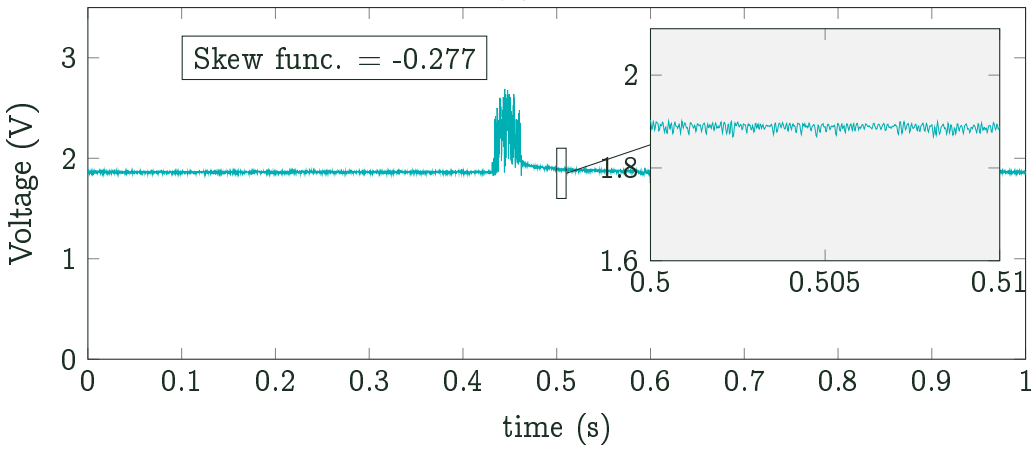

(c)

Figure 9: *Hot-film probe signal measured in plug 1 (a), 3 (b) and 5 (c) in the smooth channel of the height* $h = 1\,\mathrm{mm}$ *and* $\pi = 0.3$.

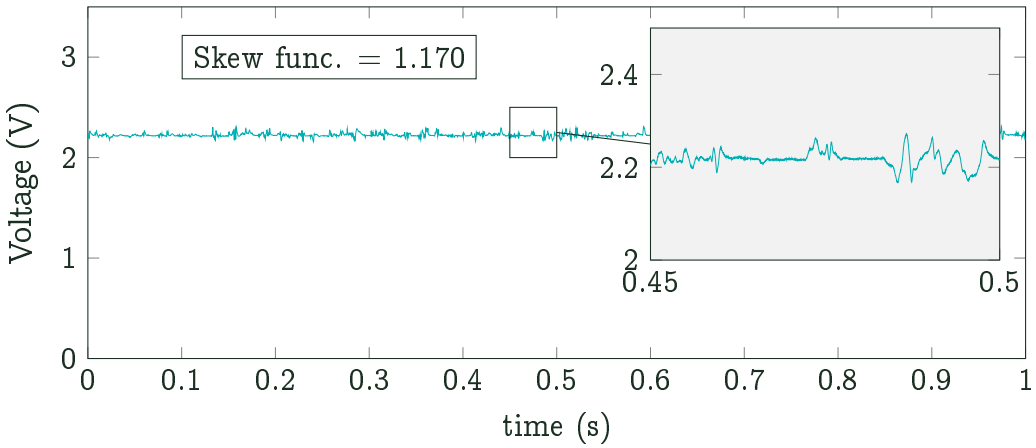

(a)

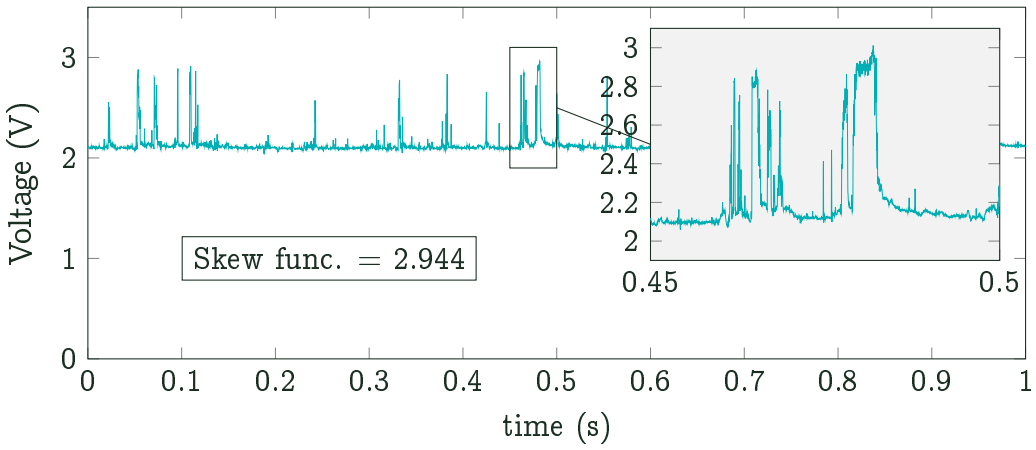

(b)

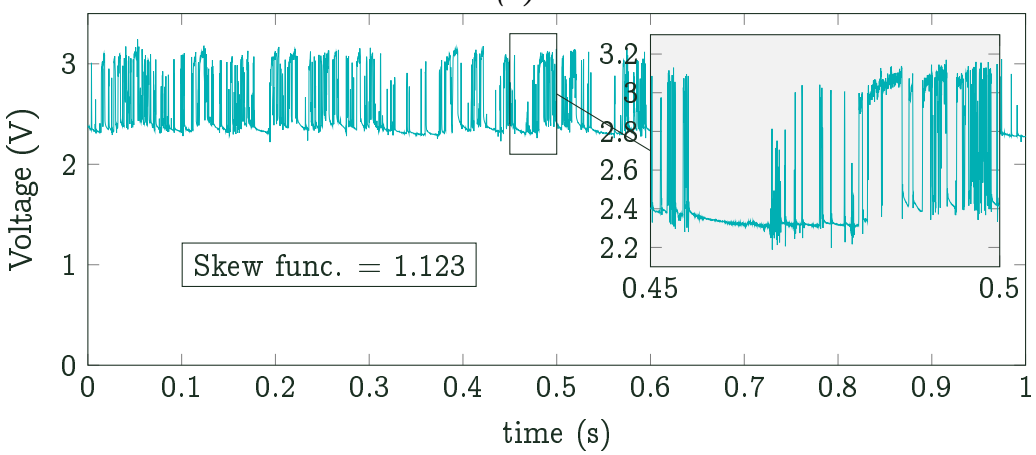

(c)

Figure 10: *Hot-film probe signal measured in plug 1 (a), 3 (b) and 5 (c) in the smooth channel of the height* $h = 2\,\mathrm{mm}$ *and* $\pi = 0.3$.

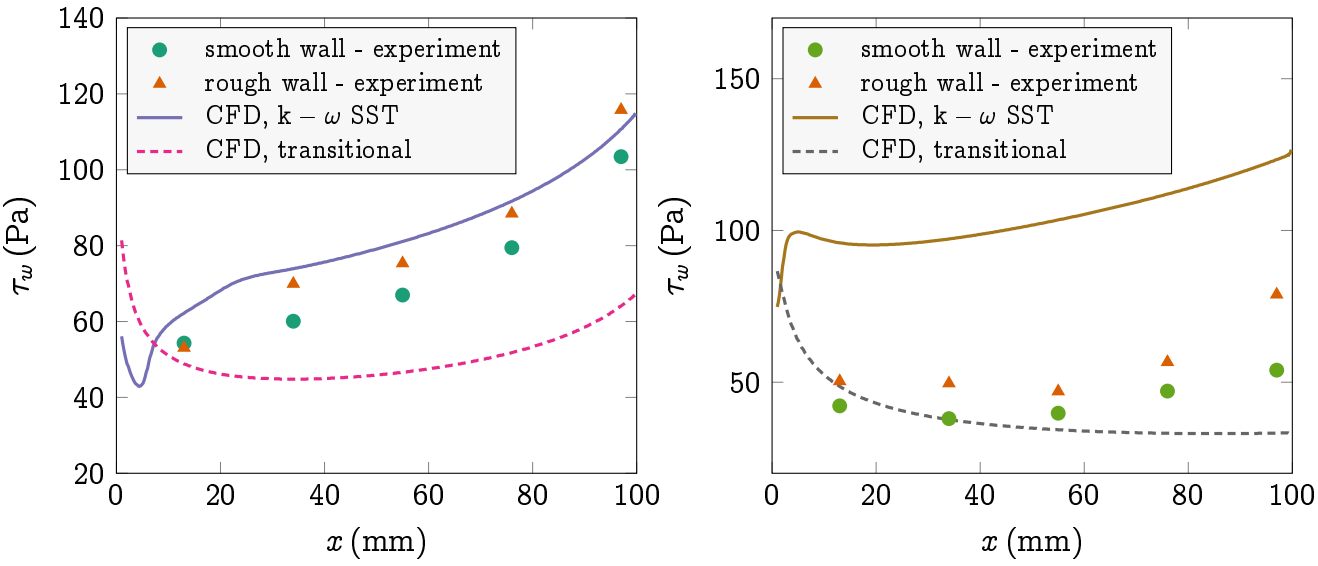

Figure 11: *Plot of the wall shear stress τ_w over the length of the channel of the height $h = 0.5\,\text{mm}$ for $\pi = 0.5$ (a) and $h = 2\,\text{mm}$ for $\pi = 0.6$ (b). Experiment and CFD values.*

in the case of channel height $h = 0.5\,\text{mm}$. In all other locations, the wall shear stress shows expected behaviour of increased values in the case of rough walls.

Comparing the measured data with computations, it can be seen that in the case of the channel height $h = 0.5\,\text{mm}$ the values computed using k – ω SST turbulence model well correspond to those measured using rough walls in both the absolute value of the wall shear stress and overall trend of the distribution, while the transitional models significantly underestimates the wall shear stress. This is most likely caused by overestimation of the entrance length by the transitional model as already illustrated using total pressure data in section 9.1.1. An important point is that computed values corresponding to smooth walls are in this case larger than the smooth wall measurements. This might question whether the use of k – ω SST turbulence model is adequate for the smooth narrow channels equipped with smooth shaped inlet part. Under such conditions the entrance length might increase and the transition to turbulence might delay leading to lower wall shear stress values than that predicted by the fully turbulent model. This problem seems to increase with increasing channel height.

As can be seen in Figure 11b, showing the case with the channel height $h = 2\,\text{mm}$, none of the used models predicts the wall shear stress satisfactorily. In this case, the better prediction over the early portion of the channel was given by transitional model and the fully turbulent one seems to significantly over-predict the wall shear stress. This is most likely caused by the fact that the flow is not yet fully developed, and as can be seen in the qualitative analysis, the mean value of the anemometer voltage, from which the wall shear stress is calculated, is in this case somewhere between fully laminar and fully turbulent value. The increased value of the wall shear stress in the case of rough wall is also in accordance with the observations of qualitative analysis which shows that the transition in the rough case is shorter resulting in higher intermittency γ i.e. higher proportion of the turbulent signal over the laminar one and thus higher mean voltage measured using hot-film probe.

The assessment of the conducted measurements and computations seems to reveal that the flow in investigated channels is for most of the regimes transitional and not fully developed

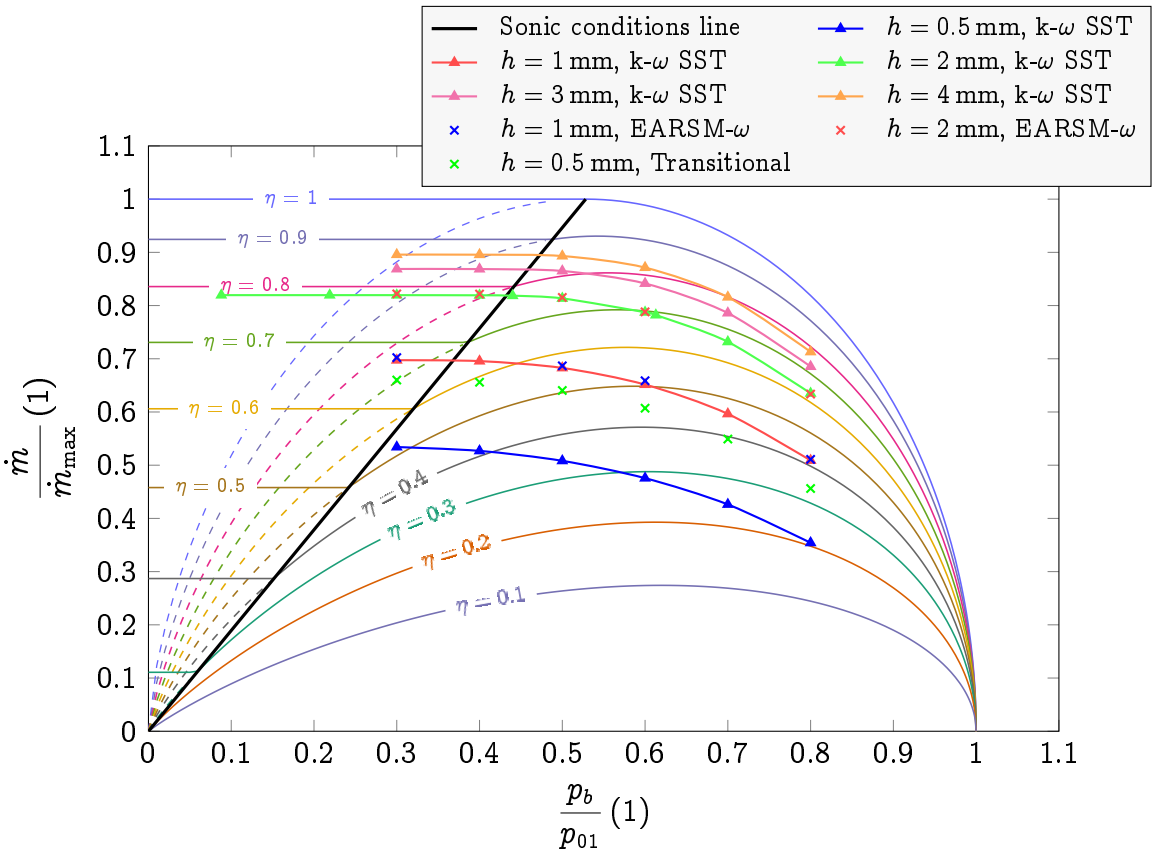

Figure 12: *Discharge diagram showing the relation between the normalized mass flow rate* $\frac{\dot{m}}{\dot{m}_{max}}$ *and back pressure ratio* $\pi = \frac{p_b}{p_{01}}$ *for constant thermodynamic efficiency* η *together with the computed expansion curves for various channel heights using different turbulence models.*

with the exception of the channel height $h = 0.5\,\text{mm}$. Only this case appeared to be fully turbulent towards the channel exit. Due to this, the fully turbulent numerical models proved not to be satisfying for wall shear stress determination and neither did the transitional model, which significantly over-predicts the entrance length.

9.2 Aerodynamic Choking Analysis

To answer the second research question, the CFD results were analysed to determine the relative mass flow rate with respect to pressure ratio. The mass flow rate $\dot{m}$ was acquired by integration throughout the exit plane of the channel while the maximum mass flow rate was calculated using the equation

$$\dot{m} = \frac{A p_0}{\sqrt{T_0}} \sqrt{\frac{\gamma}{R}} M \left(1 + \frac{\gamma - 1}{2} M^2\right)^{\frac{\gamma + 1}{2(1-\gamma)}}, \tag{7}$$

for each channel height and given boundary conditions, provided that $M = 1$, $p_0 = p_{01}$ and A is equal to channel cross section. Then, the resulting data points for each channel height were plotted in discharge diagram in Figure 12. As can be seen there, the relative mass flow rate increases with decreasing pressure ratio well beyond the ratio given by the following equation

derived in [9]

$$\left(\frac{p}{p_{01}}\right)_* = \left(z + \sqrt{z^2 + \frac{1-\eta}{\eta}\frac{2\gamma}{\gamma+1}}\right)^{\frac{\gamma}{\gamma-1}}, \tag{8}$$

where z is

$$z = \frac{1}{2\eta\,(\gamma+1)}\left[\eta\,(3\gamma+1) - 3\gamma + 1\right]. \tag{9}$$

and in fact reaches the maximum for sonic conditions given by equation

$$\left(\frac{p}{p_0}\right)_{\text{son.}} = \left[1 - \frac{\gamma-1}{\eta\,(\gamma+1)}\right]^{\frac{\gamma}{\gamma-1}}. \tag{10}$$

This can be observed for all cases except the case of $h = 0.5\,\text{mm}$, which does not yet cross the sonic conditions line even for the lowest examined pressure ratio. From this diagram it is obvious that the contradiction presented in study [9] stems from the fact that for non-ideal flow, the process of decreasing back pressure does not follow the curve of constant efficiency, which happens solely for ideal case of $\eta = 1$. It can be deduced from the plot in Figure 12 that the only way to follow the curve of constant efficiency while reducing the back pressure at the same time is by simultaneously reducing the channel height or by increasing channel length. As a result, it can be concluded that the critical condition acquired by differentiating the mass flow rate $\dot{m}$ with respect to pressure ratio $\frac{p_b}{p_0}$ and equating it to zero has very little practical importance for non-ideal flow.

To further analyse the flow choking and provide better insight in the choking process for non-ideal conditions, the relation for efficiency as a function of mass flow ratio was worked out. First, it was necessary to split the diagram to two regions. One for choked flow - left from the sonic conditions line, and the second for non-choked flow - right from the sonic conditions line. To distinguish between these two regions, it was advantageous to work out relation for sonic pressure ratio with respect to relative mass flow rate. This relation is

$$\pi_{\text{sonic}} = \frac{\dot{m}}{\dot{m}_{\max}}\left(1 + \frac{\gamma-1}{2}\right)^{\frac{\gamma}{1-\gamma}}. \tag{11}$$

Then, if the actual pressure ratio π is higher than obtained π_{sonic}, the flow is not choked and the thermodynamic efficiency can be found by solving quadratic equation

$$b^2\eta^2 - b\left[2 + \left(\frac{\dot{m}_{\max}}{\dot{m}}\right)^2 \frac{2\pi^2}{j^2(\gamma-1)}\right]\eta + 1 = 0, \tag{12}$$

where

$$b = 1 - \pi^{\frac{\gamma-1}{\gamma}} \tag{13}$$

and

$$j = \left(1 + \frac{\gamma-1}{2}\right)^{\frac{\gamma+1}{2(1-\gamma)}}. \tag{14}$$

Solving this equation gives two values of efficiency η, one of which is higher than unity. Since the solution higher than unity violates the second law of thermodynamics, only the root within the interval $\eta \in [0; 1]$ is physically possible.

If the pressure ratio π is lower than π_{sonic}, the flow is aerodynamically choked and the thermodynamic efficiency can be calculated using equation

$$\eta = \frac{\gamma - 1}{\gamma + 1} \frac{1}{1 - \pi_{\text{sonic}}^{\frac{\gamma-1}{\gamma}}}, \tag{15}$$

which yields a constant value regardless the decreasing back pressure as illustrated by solid lines of constant efficiency left of the sonic conditions line in diagram in Figure 12.

The same process plotted in $T - \Delta s$ diagram is shown in Figure 13. To plot the points there, the relation for Mach number as a function of relative mass flow rate and exit pressure ratio φ of exit plane pressure p_e to inlet total pressure p_{01}

$$\varphi = \frac{p_e}{p_{01}}, \tag{16}$$

was derived in the form of biquadratic equation

$$\left(\frac{\pi}{j}\right)^2 \frac{\gamma - 1}{2} M^4 + \left(\frac{\varphi}{j}\right)^2 M^2 - \left(\frac{\dot{m}}{\dot{m}_{\max}}\right)^2 = 0, \tag{17}$$

where j is given by equation (14). The solution of equation (17) gives two roots, from which only one is positive. Using the positive root we can obtain Mach number and subsequently the static temperature from equation

$$T = T_0 \left(1 + \frac{\gamma - 1}{2} M^2\right)^{-1}. \tag{18}$$

As in the case of discharge diagram, the special care must be taken with the points for aerodynamically choked regimes. For these points the Mach number was set to unity and the pressure ratio was taken as the sonic one for given relative mass flow rate determined by equation (11). This step, however, is not as certain as might seem because the exit Mach number might actually exceed Mach one. This phenomenon is the subject of the last research question of this thesis and will be discussed in more detail in Section 9.3.

The last thing necessary for plotting the process in $T - \Delta s$ diagram is the change of specific entropy Δs that can be calculated using relation

$$\Delta s = c_p \ln\left(\frac{T}{T_0}\right) - R \ln\left(\frac{p}{p_{01}}\right) = c_p \ln\left(\frac{T}{T_0}\right) - R \ln\left(\varphi\right), \tag{19}$$

where φ stands for the exit pressure ratio defined by equation (16).

As the $T - \Delta s$ diagram in Figure 13 shows also lines of constant thermodynamic efficiency, it can be seen again that the process of decreasing back pressure p_b does not take place at a constant efficiency. Besides that, the diagram shows also the lines of constant exit pressure ratio φ.

To conclude this part, the computational results and the analysis of the flow discharge (Figure 12) show that the actual aerodynamic choking in narrow channels occurs for pressure

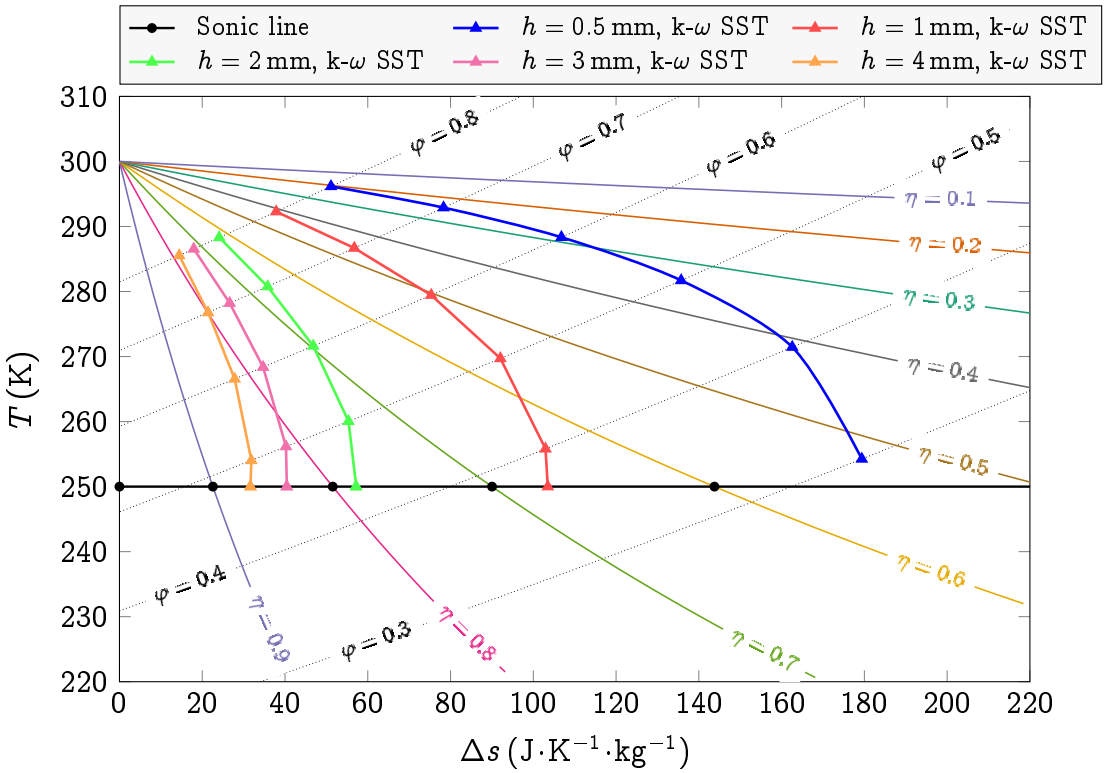

Figure 13: *Narrow channel expansion curves for various channel heights drawn in $T-\Delta s$ diagram together with lines of constant efficiency η and lines of constant exit pressure ratio φ (16).*

ratios significantly lower than for ideal case. However, the actual choking ratio can be easily predicted using equation (11) even from only one measurement or computation performed for choked regime. Nevertheless, if only one measurement is available, it is necessary to make sure that the regime was actually choked. This might be a considerable problem since with the increasing channel length or decreasing channel height, and thus with decreasing η, the actual choked pressure ratio might become unintuitively low compared with the value in the case of ideal flow as can be seen in Figure 12. For this reason, another measurement for slightly higher pressure ratio might serve as a control one. Then, if the relative mass flow rate stays constant, the flow is most likely choked and equation 12 might be used for estimation of actual choking pressure ratio. The analysis also revealed that the critical condition based on the finding of the maximum of the discharge curve for given constant thermodynamic efficiency is not applicable for non-ideal flow. Since in this case, the condition results in apparent separation of critical and sonic condition, which, however, proved to be only fictional and the governing criterion for aerodynamic choking is given by sonic condition even for non-ideal flow expressed by equation (10), provided the total pressure p_0 in this equation stands for inlet total pressure p_{01} and p for the back pressure p_b. Here it is important to note that the expression for the critical pressure ratio $\left(\frac{p}{p_0}\right)_*$ derived from the sonic condition remains valid even for non-ideal flow yielding the common formula

$$\left(\frac{p}{p_0}\right)_* = \left(\frac{2}{\gamma+1}\right)^{\frac{\gamma}{\gamma-1}}. \tag{20}$$

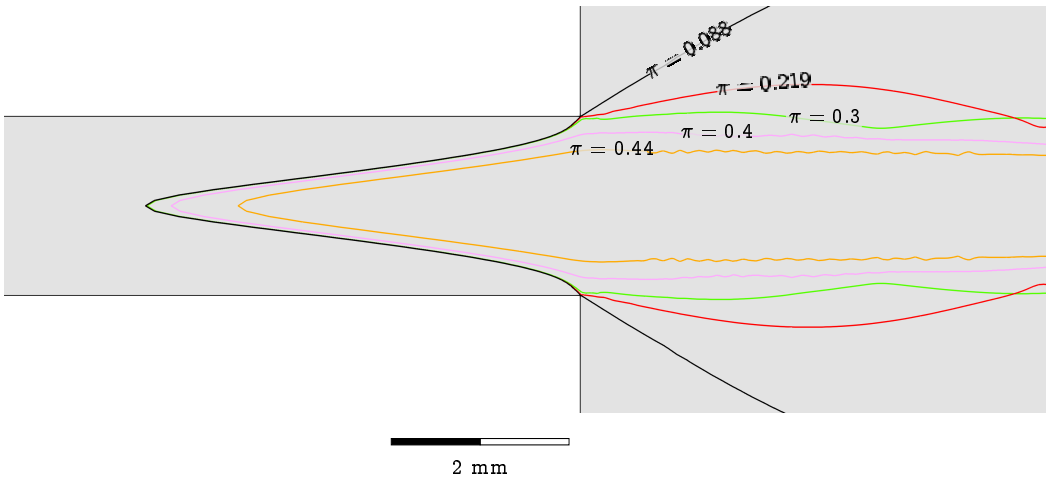

Figure 14: Sonic lines computed using $k-\omega$ *SST turbulence model in the exit part of the narrow channel of the height of* 2 mm *for various pressure ratios* π.

9.3 Flow in the Channel Exit Region

The authors of the study [10] present a hypothesis that the flow field inside the relatively long channels upstream the exit plane is affected even for the back pressure ratios significantly below the theoretical choking value represented by the sonic conditions line in Figure 12. Since this might be in contrary with the findings presented in the preceding section, which shows that the flow is indeed aerodynamically choked in terms of maximum mass flow rate for pressure ratios lower than theoretical choking value, a further analysis of the flow field focusing in particular on the channel exit region are provided in the following paragraphs.

Figure 14 shows the sonic lines (lines of Mach number $M = 1$) computed using $k-\omega$ SST turbulence model in the exit part of the narrow channel of the height of 2 mm for various pressure ratios π. The channel height of 2 mm was chosen since most of the computations and measurements were performed for this particular case. It can be seen that as the pressure ratio decreases the flow starts first to be supersonic in small region near the exit (yellow line in Figure 14). Even in this case the supersonic region extends upstream the exit plane most notably in the channel axis. Then, with further decrease of the back pressure, the supersonic region grows up until it fills the whole exit cross-section. From the regimes that have been examined, this first happen for the case with $\pi = 0.3$. For any lower π, the supersonic region inside the channel remains the same and only the flow downstream the exit plane changes as the flow must expand to reach the low pressure in the exit plenum.

Based on this examination we can say that the flow in the exit cross-section is not yet fully supersonic even for pressure ratios below approximately 0.41, for which the flow is effectively choked in terms of maximum achievable mass flow rate as can be read from diagram in Figure 12. Though, the difference is quite small. For the examined case, the difference in the length of the supersonic region is only a few tenths of a millimetre.

Another question is the course of displacement thickness along the channel. Lio et al. claim that the boundary layer might narrow in the very vicinity of the exit plane forming divergent nozzle-like shape, which causes the acceleration of the flow beyond $M = 1$. Therefore, the

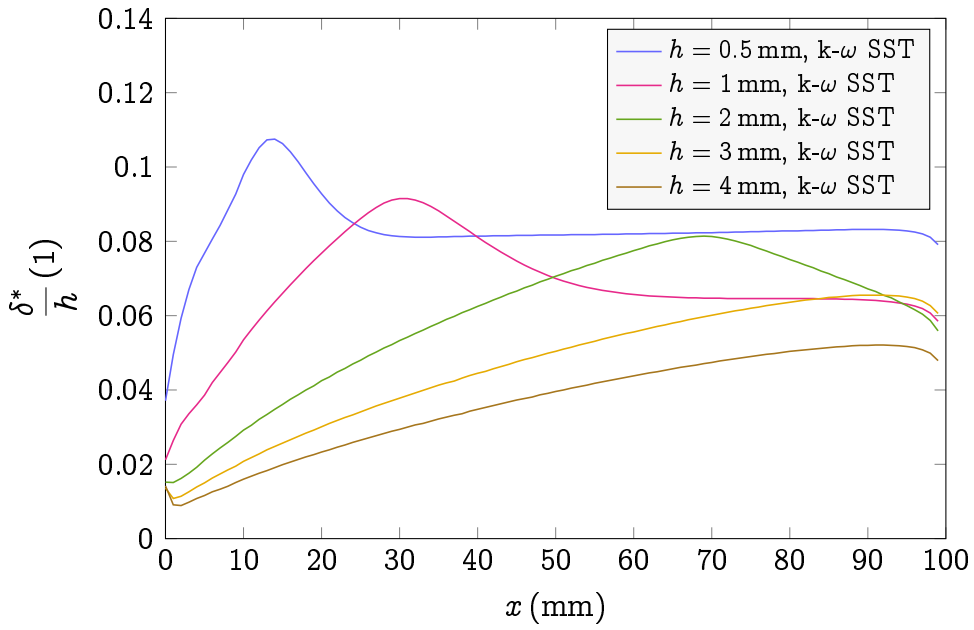

Figure 15: *Normalised displacement thickness* $\frac{\delta^*}{h}$ *along the channel for various channel heights and pressure ratio* $\pi = 0.3$ *as computed using k-ω SST turbulence model.*

displacement thickness defined as

$$\delta^*(x) = \int_0^{\frac{h}{2}} \left(1 - \frac{\rho(x,y)u(x,y)}{\rho_e u_e(x)}\right) \mathrm{d}y, \tag{21}$$

was calculated for some regimes. The h in the equation above stands for channel height and ρ_e and u_e are mid channel density and velocity respectively. The results of this analysis showing the course of displacement thickness for pressure ratio $\pi = 0.3$ and various channel heights can be seen in Figure 15. It can be best observed on the case of $h = 0.5$ mm that the displacement thickness initially grows up than reduces and keeps at approximately constant value up to very vicinity of the channel exit where another drop occurs. The first drop most likely corresponds to vanishing of the inviscid core in the flow and thus is related to flow development. Based on this, we can say that the flow in this CFD study is probably fully developed only in the case of $h = 0.5$ and $h = 1$ mm, which exhibits the plateau after initial growth and subsequent drop. Nevertheless, in all cases another drop in displacement thickness is apparent near the exit, which might cause the flow to accelerate beyond $M = 1$ as was predicted in study by Lio et al. Even though, the raw hot-film probe data discussed in qualitative analysis show some sort of signal flattening probably due to high favourable pressure gradient causing rapid flow acceleration in the location of the last measuring plug, neither quantitative measurements nor computations confirmed reduction of the wall shear stress close to the channel exit, which was discussed in [4]. It is indeed necessary to mention that it was not possible to conduct the quantitative measurements for pressure ratio π lower than approximately 0.5, therefore, to fully address this issue additional measurements should be performed.

10 Conclusions

This section summarizes the conclusions drawn from the research conducted during the entire doctoral project. The main objective of this project was to explore the nature of the flow in narrow channels and investigate the influence of two different types of surface roughness particularly on the flow development and the wall shear stress distribution along the channel. This part was preceded by an extensive set of tests on the calibration facility followed by the numerical investigations, which together led to calibration of the hot-film probe representing one of the few promising methods to measure the wall shear stress in such a confined geometries. Yet, not easy to use due to many shortcomings, which had to be overcome before actual measurements. The second objective was to find out whether the flow in narrow channels experiences the separation of sonic conditions from critical conditions due to friction as theoretically predicted in study [9]. This was accomplished mostly using theoretical analyses and numerical simulations, which also provided further insight into the narrow channel flow and helped to answer the third research question that was whether the flow in the exit region of the narrow channels might experience reduction in the wall shear stress and the thinning of the boundary layer.

To answer the first research question, the results of the RANS numerical simulations using both fully turbulent and transitional turbulence models were compared to the results of a number of experimental methods. These included pneumatic measurements, optical measurements (interferometry) and hot-film anemometry. The most valuable results were obtained using the hot-film probe, which proved to be an effective method to identify the state of the flow. Further, after the calibration, the hot-film probe was also successfully used to measure the wall shear stress. The analysis of the results revealed that the flow in the examined channels was for most of the investigated channel heights transitional and not fully developed. As a result, the wall shear stress distribution was not captured satisfactorily with none of the used numerical models with the exception of the channel height $h = 0.5\,\mathrm{mm}$ with cross-flow roughness, in which case the fully turbulent model provided satisfying results. Another important finding was that the total pressure measurements in the mid channel close to channel exit provided well comparable results to the fully turbulent numerical simulations for all examined cases yielding a good estimate of the total pressure loss. However, as apparent from the qualitative hot-film probe measurements a good estimate of the total pressure loss does not guarantee reliable prediction of the distribution of the wall shear stress. It also proved that one-dimensional approach to determine the friction factor in the case of relatively short channels is barely usable and provides the friction factor values by more than order of magnitude lower than what should correspond to actually measured wall shear stress [A6], which is in agreement with the observations referenced in [20]. Overall, the analyses of the raw hot-film probe signal and subsequent analysis of the signal skewness together with the quantitative measurements proved to be capable to provide substantial information about the nature of the flow, which is important for validation of numerical models [A3][A2][A7]. Such analyses revealed that both examined types of surface roughness shorten the transition and increase the absolute values of the wall shear stress. At the same time, the streamwise roughness apparently increases the effective channel cross-section, which is more pronounced with decreasing channel height. At this point it is important to note that the quantitative analysis itself provides only mean value of the wall shear stress at the measuring location and thus the further analyses of the

raw signal should always follow to obtain an information whether the flow is developed or transitional and, in the later case, in which stage of transition it is.

The second objective was accomplished by theoretical analysis and accompanying numerical study. The analysis revealed that the actual choking occurs for non-ideal flow for lower values of the driving pressure ratio π. However, the choking takes place when the sonic pressure ratio is reached in the critical cross-section. Therefore, equation (10) can be used for determination of the actual back pressure ratio π necessary for given thermodynamic efficiency η to obtain aerodynamically choked flow. Additionally, the working formulas for mass flow rate ratio with respect to back pressure ratio and thermodynamic efficiency as a parameter were derived and the resulting relations were drawn together with the results of the numerical simulations in more comprehensive form in charts in Figure 12 and in the $T - \Delta s$ diagram in Figure 13.

The numerical simulations were also used to explore the flow close to the channel exit revealing that the sonic line actually moves inwards the channel even for pressure ratios, below which the flow is aerodynamically choked. Nevertheless, this change was quite small and seems to have negligible influence on the resulting mass flow rate through the channel, therefore, the choking condition expressed by the maximum of the mass flow rate remains satisfied. The numerical computations also proved that the boundary layer is thinning close to the channel exit most likely due to large favourable pressure gradient as also referenced in study [10]. However, despite the observable influence on the hot-film probe signal, which apparently flattened indicating diminishing of the turbulent fluctuations, both quantitative measurements and computations yield increasing wall shear stress towards the channel exit. Yet, the quantitative measurements were not conducted for choked flow regime, which would require back pressure ratio lower than approximately $\pi = 0.3$ in the case of channel height $h = 0.5\,\mathrm{mm}$, therefore, additional measurements can be recommended to explore the influence of even larger pressure gradients, which will be a subject of following research.

As a final conclusion it can be said that all three main objectives of this thesis were successfully achieved as well as a number of additional tasks which emerged during the course of this project. Furthermore, despite the complicated calibration, the hot-film anemometry turned out to be powerful method, which together with other methods already well established in our laboratory, has potential to substantially enhance the capability in investigation of the compressible viscous flow and demonstrated its potential not only for the investigation of confined geometries such as narrow channels but also for compressor and turbine blade cascades as already demonstrated during the measurements on the transonic blade profile [A4]. This is of particular importance since compressor and turbine blades still represent the most common test articles in Nový Knín laboratory.

References

Author's Publications Related with the Present Thesis

A1. HÁLA, J. *Compressible Fluid Flow through Minichannel*. Prague: Master Thesis, CTU in Prague, Faculty of Mechanical Engineering, 2014.

A2. PRAUSOVÁ, H.; BUBLÍK, O.; VIMMR, J.; LUXA, M.; HÁLA, J. Clearance gap flow: Simulations by Discontinuous Galerkin Method and Experiments. *EPJ Web of Conferences*. 2015, vol. 92. Available from DOI: 10.1051/epjconf/20159202073.

A3. HÁLA, J.; LUXA, M.; PRAUSOVÁ, H.; BUBLÍK, O.; VIMMR, J. Clearance Gap Flow: Extended Pneumatic Measurements and Simulations by Discontinuous Galerkin Finite Element Method. *EPJ web of conferences*. 2016, vol. 114. Available from DOI: 10.1051/epjconf/201611402034.

A4. LUXA, M.; HÁLA, J. *Measurements on NACA 0010-64 profile*. Prague, 2018. Research report, Z-1596/18. Institute of Thermomechanics of the Czech Academy of Sciences.

A5. HÁLA, J.; LUXA, M. Numerical and Experimental Studies of the Flow Through Narrow Gap. In: *Colloquium Fluid Dynamics 2014 Proceedings*. Prague, 2014, pp. 15–16.

A6. HÁLA, J.; LUXA, M.; BUBLÍK, O.; PRAUSOVÁ, H.; VIMMR, J. Compressible Viscous Flow in Minichannel - Experiment and Numerical Studies. In: *Computational Mechanics 2014 - Book of extended abstracts*. Pilsen, 2014, pp. 39–40.

A7. PRAUSOVÁ, H.; BUBLÍK, O.; VIMMR, J.; HÁLA, J.; LUXA, M. Numerical and Experimental Investigation of Compressible Viscous Fluid Flow in Minichannels. In: *Proceedings of Computational mechanics 2019*. Pilsen, 2019, pp. 160–163.

Other References

1. AVILA, K.; MOXEY, D.; LOZAR, A. de; AVILA, M.; BARKLEY, D.; HOF, B. The Onset of Turbulence in Pipe Flow. *Science*. 2011, vol. 333, no. 6039, pp. 192–196. Available from DOI: 10.1126/science.1203223.

2. ECKHARDT, B.; SCHNEIDER., T. M.; HOF, B.; WESTERWEEL, J. Turbulence Transition in Pipe Flow. *Annual Review of Fluid Mechanics*. 2007, vol. 39, no. 1, pp. 447–468. Available from DOI: 10.1146/annurev.fluid.39.050905.110308.

3. DIXIT, T.; GHOSH, I. Review of micro- and mini-channel heat sinks and heat exchangers for single phase fluids. *Renewable and Sustainable Energy Reviews*. 2015, vol. 41, pp. 1298–1311. Available from DOI: https://doi.org/10.1016/j.rser.2014.09.024.

4. LUXA, M.; DVOŘÁK, R.; ŠIMURDA, D.; VIMMR, J. Gas Flow in Constant Area Minichannels. In: *10th International Symposium on Experimental and Computational Aerothermodynamics of Internal Flows - ISAIF 10*. Vrije Universiteit Brussel, 2011, pp. 52–58.

5. VIMMR, J.; KLÁŠTERKA, H.; HAJŽMAN, M.; LUXA, M.; DVOŘÁK, R. Mathematical modelling and experimental investigation of gas flow in minichannels and microchannels. *Journal of Thermal Science*. 2010, vol. 19, pp. 289–294. Available from DOI: 10.1007/s11630-010-0385-x.

6. SHAPIRO, A. H. *The Dynamics and Thermodynamics of Compressible Fluid Flow. Vol. I.* The Ronald Press Company, 1953.
7. MLYNAŘÍKOVÁ, H. *Mathematical modeling of turbulent flows.* Pilsen: Master Thesis, University of West Bohemia, Faculty of Applied Sciences, 2012. (in Czech).
8. PRAUSOVÁ, H. *Modelling of turbulent flows using RANS and implicit LES with application of discontinuous Galerkin method.* Pilsen: Ph.D. Thesis, University of West Bohemia, Faculty of Applied Sciences, 2019. (in Czech).
9. HYHLÍK, T.; J.MACEK; P.ŠAFAŘÍK. A Contribution to Solution of Aerodynamic Choking in Flow Parts of Machines at Consideration of Thermodynamic Efficiency. In: *Colloquium FLUID DYNAMICS 2001.* Prague, 2001, pp. 23–26. (in Czech).
10. LIJO, V.; KIM, H. D.; SETOGUCHI, T. Analyses of Choked Viscous Flows Through a Constant Area Ducts. In: *Proceedings of the Institution of Mechanical Engineers.* 2010, vol. 224, G11.
11. MACMILLAN, F. A. *Experiments on Pitot-tubes in Shear Flow.* London, 1957. Technical Report, No. 3028. Aeronautical Research Council, Reports and Memoranda.
12. *NetScanner™System 9116.* Hampton, VA, 2012. Available from `http://www.measspec.com/register.aspx?id=9235#`.
13. PŘÍHODA, J. *Methods of Wall-Shear Stress Measurements.* Prague, 1974. Research Report, Z-443/74. Institute of Thermomechnics AS CR, v.v.i. (in Czech).
14. LIEPMNANN, H. W.; SKINNER, G. T. *Shearing Stress Measurements by Use of a Heated Element: Technical note 3268.* 1954. Technical note 3268. California Institute of Technology.
15. TROPEA, C.; YARIN, A.; FOSS, J. F. (eds.). *Handbook of Experimental Fluid Mechanics.* Berlin Heidelberg: Springer-Verlag, 2007.
16. HODSON, H. P.; HUNTSMAN, I. I.; STEELE, A. B. An Investigation of Boundary Layer Development in a Multistage LP Turbine. In: *Proceedings of ASME Turbo Expo 1993: Power for Land, Sea and Air.* Cincinatti, Ohio, 1993. No. 93-GT-310.
17. TIEDEMANN, M.; KOST, F. Unsteady Boundary Layer Transition on a High Pressure Turbine Rotor Blade. In: *Proceedings of ASME Turbo Expo 1993: Power for Land, Sea and Air.* Indianapolis, Indiana, 1999. No. 99-GT-194.
18. ROACHE, P. J. Quantification of uncertainty in computational fluid dynamics. *Annual Review of Fluid Mechanics.* 1997, vol. 29, no. 1, pp. 123–160. Available from DOI: 10.1146/annurev.fluid.29.1.123.
19. FITZGERALD, J. E.; NIVEN, A. J.; DAVIES, M. R. D. Turbine Blade Aerodynamic Wall Shear Stress Measurements and Predictions. In: *Proceedings of ASME Turbo Expo 1998: Power for Land, Sea and Air.* Stockholm, Sweden, 1998. No. 98-GT-562. Available from DOI: 10.1115/98-GT-562.
20. SHAPIRO, A. H. *The Dynamics and Thermodynamics of Compressible Fluid Flow. Vol. II.* The Ronald Press Company, 1954.